Skyrmion Qubits: A New Class of Quantum Logic Elements Based on Nanoscale Magnetization

Christina Psaroudaki[1,2,*] and Christos Panagopoulos[3,†]

[1]*Department of Physics and Institute for Quantum Information and Matter,*
California Institute of Technology, Pasadena, California 91125, USA
[2]*Institute for Theoretical Physics, University of Cologne, D-50937 Cologne, Germany*
[3]*Division of Physics and Applied Physics, School of Physical and Mathematical Sciences,*
Nanyang Technological University, 21 Nanyang Link 637371, Singapore

We introduce a new class of primitive building blocks for realizing quantum logic elements based on nanoscale magnetization textures called skyrmions. In a skyrmion qubit, information is stored in the quantum degree of helicity, and the logical states can be adjusted by electric and magnetic fields, offering a rich operation regime with high anharmonicity. By exploring a large parameter space, we propose two skyrmion qubit variants depending on their quantized state. We discuss appropriate microwave pulses required to generate single-qubit gates for quantum computing, and skyrmion multiqubit schemes for a scalable architecture with tailored couplings. Scalability, controllability by microwave fields, operation time scales, and readout by nonvolatile techniques converge to make the skyrmion qubit highly attractive as a logical element of a quantum processor.

Quantum computing promises to dramatically improve computational power by harnessing the intrinsic properties of quantum mechanics. Its core is a quantum bit (qubit) of information made from a very small particle such as an atom, ion, or electron. Proposed qubit systems include trapped atoms, quantum dots, and photons [1–3]. Among them, superconducting circuits, currently one of the leading platforms for noisy intermediate-scale quantum computing protocols [4], are macroscopic in size but with well-established quantum properties [5]. Nevertheless, despite tremendous progress, significant challenges remain, in particular with respect to control and scalability [6].

Here we propose an alternative macroscopic qubit design based on magnetic skyrmions, topologically protected nanoscale magnetization textures, which have emerged as potential information carriers for future spintronic devices [7]. We focus on frustrated magnets, in which skyrmions and antiskyrmions have a new internal degree of freedom associated with the rotation of helicity [8–12]. In these systems, the noncollinear spin texture induces electric polarization, allowing for electric-field modulation of the skyrmion helicity [13,14]. Along with magnetic field gradients [15] (MFGs) and microwave fields [16,17], electric fields emerge as a new, powerful tool for a current-free control of skyrmion dynamics [18]. Skyrmions of a few lattice sites [19] inspired theoretical studies on their quantum properties [20,21]. Similar to Josephson junctions [22,23], their macroscopic quantum tunneling and energy-level quantization are indicative of quantum behavior. In sufficiently small magnets, an analogous quantum behavior in terms of macroscopic quantum

tunneling of the magnetic moment has been experimentally verified in mesoscopic magnetic systems [24–26], while the quantum depinning of a magnetic skyrmion has been theoretically proposed [27].

We formulate a theoretical framework of skyrmion quantization and construct skyrmion qubits based on the energy-level quantization of the helicity degree of freedom. The ability to control the energy-level spectra with external parameters, including electric and magnetic fields, offers a rich parameter space of possible qubit variants with high anharmonicity and tailored characteristics. We propose microwave MFGs for skyrmion qubit manipulation and gate operation, and consider skyrmion multiqubit schemes for a scalable architecture. A skyrmion qubit has a moderately high coherence time in the microsecond regime, while nonvolatile readout techniques can be employed for a reliable qubit state readout. Finally, we discuss how scale-up multiqubit challenges can be addressed by leveraging state-of-the-art skyrmion technology and show that skyrmion qubits are suitable for quantum computing technology.

Skyrmion field quantization.—We begin by considering the inversion-symmetric Heisenberg model with competing interactions [10],

$$\mathcal{F} = -\frac{J_1}{2}(\nabla \mathbf{m})^2 + \frac{J_2 a^2}{2}(\nabla^2 \mathbf{m})^2 - \frac{H}{a^2}m_z + \frac{K}{a^2}m_z^2, \quad (1)$$

where H and K are the Zeeman and anisotropy coupling, respectively, while J_1 and J_2 denote the strength of the competing interactions and a the lattice spacing. A number
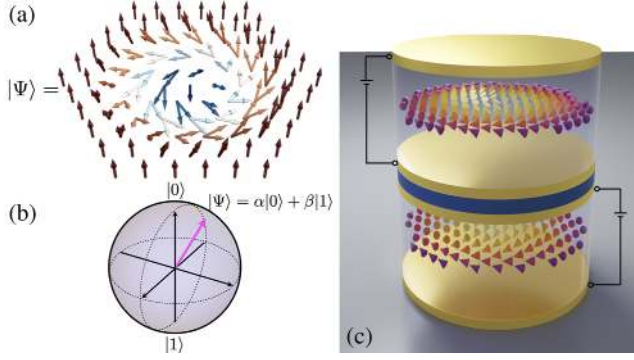
FIG. 1. Skyrmion qubit concept. (a) A quantum state $|\Psi\rangle$ as an arbitrary superposition of skyrmion configurations with distinct helicities φ_0. (b) Bloch sphere representation of $|\Psi\rangle = \alpha|0\rangle + \beta|1\rangle$, with $|0\rangle$ and $|1\rangle$ denoting the two lowest energy levels of the quantum operator $\hat{\varphi}_0$. (c) A bilayer of magnetic materials as a platform for the skyrmion qubit coupling scheme. The qubit coupling is tuned by a nonmagnetic spacer (blue), and logical states are adjusted by electric fields (yellow plates).

of geometrically frustrated magnets are good candidates to host complex spin textures [8], including the triangular-lattice magnet Gd_2PdSi_3, known to support skyrmion phases [28]. Using $\mathbf{m} = [\sin\Theta\cos\Phi, \sin\Theta\sin\Phi, \cos\Theta]$, we describe classical skyrmions by $\Phi(\mathbf{r}) = -Q\phi$ and $\Theta = \Theta(\rho)$, with ρ, ϕ polar coordinates. This class of solutions is characterized by an integer-valued topological charge $Q = (1/4\pi)\int_{\mathbf{r}} \mathbf{m}\cdot(\partial_x\mathbf{m}\times\partial_y\mathbf{m})$, with $Q = 1$ ($Q = -1$) for a skyrmion (antiskyrmion). The skyrmion size is defined as $\lambda \equiv 2a/\text{Re}[\gamma_\pm]$, with $\gamma_\pm = \sqrt{-1\pm\tilde{\gamma}}/\sqrt{2}$ and $\tilde{\gamma} = \sqrt{1 - 4(H/J_1 + 2K/J_1)}$. The model of Eq. (1) has an unbroken global symmetry, $\Phi \to \Phi + \varphi_0$, with φ_0 the collective coordinate of the skyrmion helicity. By considering a skyrmion stabilized in a nanodisk (see Fig. 1), we exclude the translational coordinate of position [21] and focus exclusively on the dynamics of φ_0.

To investigate quantum effects, we utilize a method of collective coordinate quantization. Here φ_0 and its conjugate momentum S_z are introduced by performing a canonical transformation in the phase space path integral [29,30] (see Supplemental Material [31]). This is achieved by ensuring momentum is conserved, $S_z = P$, with $P = \int_{\mathbf{r}}(1 - \cos\Theta)\partial_\phi\Phi$ the infinitesimal generator of rotations satisfying $\{P, \Phi\} = -\partial_\phi\Phi$. Using standard equivalence between path integral and canonical quantization, we introduce operators $\hat{\varphi}_0$ and $\hat{S}_z$ with $[\hat{\varphi}_0, \hat{S}_z] = i/\bar{S}$, and $\bar{S}$

the effective spin. The classical limit is associated with $\bar{S} \gg 1$. Eigenstates of $\hat{S}_z$ are labeled by an integer charge s with $\hat{S}_z|s\rangle = s/\bar{S}|s\rangle$, and states $\hat{\varphi}_0|\varphi_0\rangle = \varphi_0|\varphi_0\rangle$ have a circular topology $|\varphi_0\rangle = |\varphi_0 + 2\pi\rangle$. The relation between physical and dimensionless parameters is summarized in Table I. We construct skyrmion qubits based on textures with $Q = 1$. Antiskyrmion qubits follow directly from our present analysis.

Fundamental skyrmion qubit types.—We now seek to construct a skyrmion qubit based on the energy-level quantization of the helicity degree of freedom. A promising qubit candidate needs to satisfy several criteria including scalability, ability to initialize to a simple fiducial state, long decoherence times, a universal set of quantum gates, and the ability to perform qubit-specific measurements [32].

The S_z qubit: The ability to control the energy-level spectra with external parameters, offers a rich parameter space of possible qubit variants with tailored characteristics. We introduce the S_z-qubit Hamiltonian,

$$H_{S_z} = \kappa(\hat{S}_z - h/\kappa)^2 - E_z\cos\hat{\varphi}_0, \tag{2}$$

which resembles the circuit Hamiltonian of a superconducting charge qubit [33]. Here κ and h denote the anisotropy and magnetic field coupling, respectively, in dimensionless units. The noncollinear spin texture gives rise to an electric polarization which couples to an electric field E_z applied across the nanodisk to control φ_0 [14] (see Fig. 1 for a schematic illustration of the setup). The S_z qubit is designed in the $E_z \ll \kappa$ regime, such that logical qubits are spin states $|s\rangle$, representing deviations of the m_z component from equilibrium. The solution of the Schrödinger equation $H_{S_z}\Psi_s(\varphi_0) = \mathscr{E}_s\Psi_s(\varphi_0)$, with $\Psi_s(\varphi_0) = \langle\varphi_0|s\rangle$, can be calculated exactly in the form of special functions (see Supplemental Material [31]). In Fig. 2(b) we plot the potential landscape and the first three levels using $\kappa = 0.1$, $h = 0.47$, and $E_z = 0.02$.

Two requirements are essential for a reliable qubit operation; nonequidistance of the energy spectrum to uniquely address each transition and suppressed spontaneous thermal excitations to higher energy levels $k_B T \ll \hbar\omega_{12}$, $\hbar\omega_{02}$. The remarkable feature of skyrmion qubits is that these conditions can be met by tuning the relevant external parameters. In Fig. 2(a) we present the range of parameters $\bar{h} = h\bar{S}/\kappa$ and E_z for which a relatively large anharmonicity is present, $|\omega_{12} - \omega_{01}| > 20\%\omega_{01}$ and $|\omega_{02} - \omega_{01}| > 20\%\omega_{01}$.

TABLE I. Relation between physical and dimensionless parameters. We use $J_1 = 1$ meV, $a = 5$ Å, $\bar{S} = 10$, $J_2 = J_1$, $K = 0.4J_1$, $K_x = 0.05J_1$, and $P_E = 20$ μC/cm^2. MFG stands for magnetic field gradient.

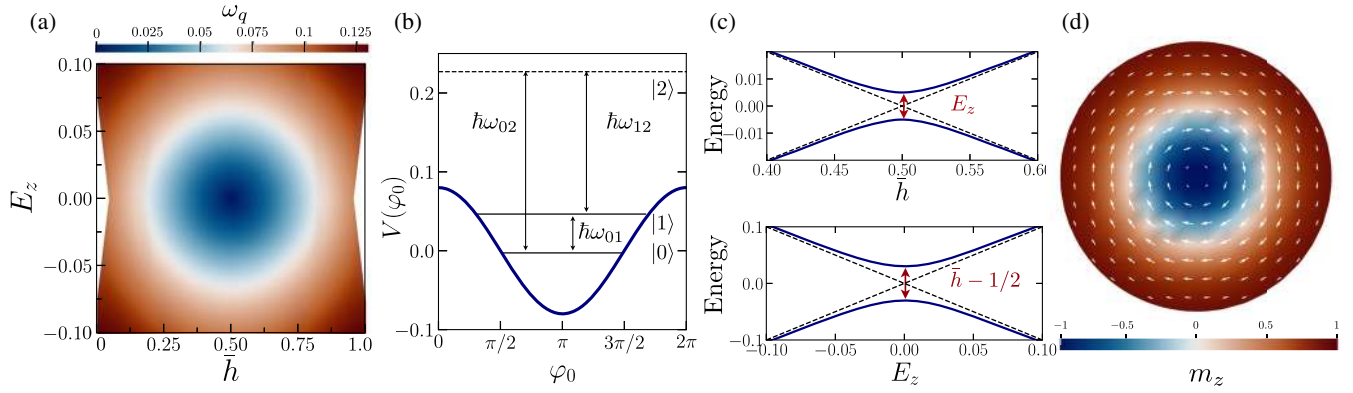| Length	Time	Frequency	Temperature	Magnetic field	Electric field	Static MFG
$\mathbf{r} \times 0.5$ nm	$t \times 6.6 10^{-13}$ s	$\omega \times 1519$ GHz	$T \times 11.6$ K	$H/g\mu_B = h \times 0.86$ T	$E = E_z \times 215$ V/m	$H_\perp/g\mu_B = h_\perp \times 1.72$ T/nm

FIG. 2. The S_z-qubit properties. (a) Magnetic field $\bar{h}$ and electric field E_z dependence of the transition frequency ω_q, close to the degeneracy point $\bar{h} = 0.5$. The colored surface represents the values of ω_q which satisfy the requirement of high anharmonicity. (b) Nonequidistant quantized energy levels and potential landscape. The qubit states are the ground state $|0\rangle$ and first excited state $|1\rangle$ with level spacing $\hbar\omega_{01} = \omega_q$ smaller than transitions to higher states $\hbar\omega_{02}$, $\hbar\omega_{12}$. (c) Universal energy level anticrossing diagram close to the degeneracy point (dashed lines). The degeneracy is lifted by an electric field (upper panel) or increasing the magnetic field away from $\bar{h} = 0.5$ (lower panel). At the degeneracy point, energy eigenstates are symmetric and antisymmetric superpositions of the skyrmion qubit states $(|0\rangle \pm |1\rangle)/\sqrt{2}$. (d) A magnetic skyrmion with a circular profile stabilized in a magnetic nanodisk.

For $\bar{h} = 1/2$, the two lowest spin states $|0\rangle$ and $|1\rangle$ are degenerate, and a small E_z lifts the degeneracy creating a tight two-level system. Truncating the full Hilbert space to qubit subspace, the reduced Hamiltonian is

$$H_q = \frac{H_0}{2}\hat{\sigma}_z - \frac{X_c}{2}\hat{\sigma}_x, \qquad (3)$$

with $H_0 = \kappa(1 - 2\bar{h})/\bar{S}$, $X_c = E_z$, and $\omega_q = \sqrt{H_0^2 + X_c^2}$ the corresponding qubit level spacing. The universal level repulsion diagram is shown in Fig. 2(c), with a minimum energy splitting E_z. The S_z-qubit operation regime in physical units is given in Table II. We note that the proposed qubit platform has large anharmonicity, and the voltage bias for qubit manipulation is several orders of magnitude smaller compared to those required for the electric-field skyrmion creation and annihilation [18].

The helicity qubit: Inspired by the superconducting flux qubit and proposals on magnetic domain walls [34], we seek to construct a double-well potential landscape for the helicity φ_0, in order to define the qubit logical space using the two well minima. This is achieved by considering a material with in-plane magnetic anisotropy of strength κ_x [35] and a skyrmion characterized by an elliptical profile, as the result of defect engineering [36,37]. The Hamiltonian

for this new type of helicity qubit reads $H_{\varphi_0} = \kappa\hat{S}_z - h\hat{S}_z + V(\hat{\varphi}_0)$, with the double-well potential given by

$$V(\varphi_0) = \kappa_x \cos 2\hat{\varphi}_0 - E_z \cos \hat{\varphi}_0 + h_\perp \sin \hat{\varphi}_0. \qquad (4)$$

The first two terms in Eq. (4) create a symmetric potential, and the third term describes a depth difference between the well created by an in-plane MFG of strength $h_\perp$. The solutions of the eigenvalue problem $1H_{\varphi_0}\Psi_n(\varphi_0) = \mathscr{E}_n\Psi_n(\varphi_0)$ are 2π-periodic functions calculated numerically. The potential in the helicity representation is schematically shown in Fig. 3(b) together with the first three levels. Close to the degeneracy point at $\bar{h} = 1$ and for $h_\perp = 0$, the two lowest energy functions $\Psi_{0,1}$ are symmetric and antisymmetric combinations of the two wave functions localized in each well located at $\varphi_m = \tan^{-1}(\sqrt{16\kappa_x^2 - E_z^2}/E_z)$. A finite $h_\perp$ acts as an energy bias creating a depth well difference, such that the ground and first-excited states are now localized in different wells.

At $\bar{h} = 1$, level anticrossing can be probed by applying either an electric field E_z [see Fig. 3(c), upper panel] or a magnetic field gradient $h_\perp$ [see Fig. 3(c), lower panel]. The

TABLE II. Skyrmion qubit operation regime and lifetime. We use $\alpha = 10^{-5}$ and $T = 100$ mK. EF stands for electric field and MFG for magnetic field gradient.

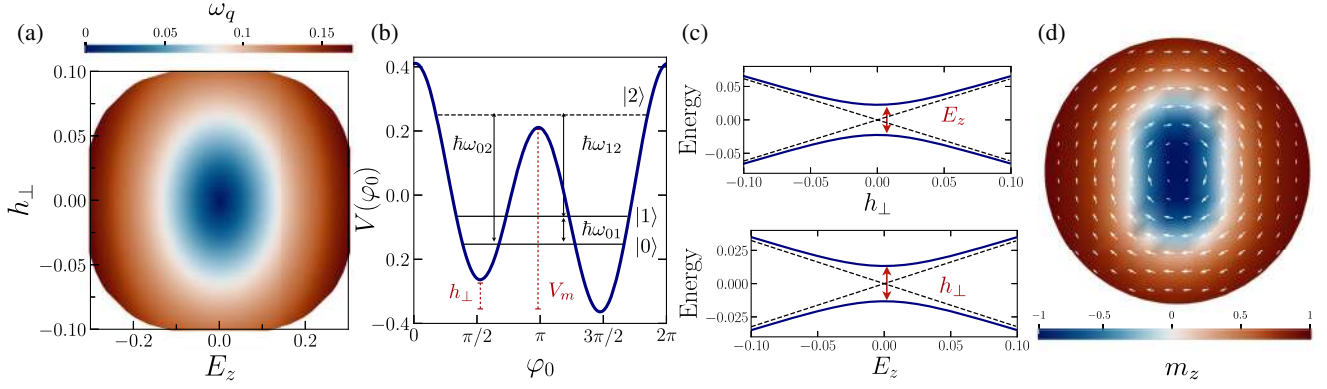| Qubit type	Magnetic field	External control	ω_q	T_1	T_2	ω_{12}	T_c
S_z qubit	8.9 mT	EF = 108 mV/μm	25.6 GHz	0.27 μs	0.49 μs	310 GHz	2.50 K
Helicity qubit	445 mT	EF = 296 mV/μm	14.9 GHz	0.15 μs	0.26 μs	330 GHz	2.60 K
Helicity qubit	445 mT	MFG = 1.73 mT/nm	2.1 GHz	0.43 μs	0.32 μs	330 GHz	2.55 K

FIG. 3. The helicity-qubit properties. (a) Electric field E_z and magnetic field gradient $h_\perp$ dependence of the transition frequency ω_q, close to the degeneracy point $\bar{h} = 1$. The colored surface represents the values of ω_q which satisfy the requirement of high anharmonicity. (b) Nonequidistant quantized energy levels and double-well potential landscape. The qubit states are the ground state $|0\rangle$ and first excited state $|1\rangle$ with level spacing $\hbar\omega_{01} = \omega_q$ smaller than transitions to higher states $\hbar\omega_{02}$, $\hbar\omega_{12}$. The potential barrier V_m is controlled by E_z and the well difference by $h_\perp$. (c) Universal energy level anticrossing diagram close to the degeneracy point $\bar{h} = 1$. The degeneracy is lifted by an electric field (upper panel) or a magnetic field gradient (lower panel). (d) A magnetic skyrmion with an elliptical profile stabilized in a magnetic nanodisk. The elliptical profile is essential for realizing the double-well potential.

reduced qubit Hamiltonian under the two-level approximation has the form of Eq. (3), where $H_0 = \mathcal{E}_1 - \mathcal{E}_0$ and $X_c = g_e E_z$ for $h_\perp = 0$, or $X_c = g_b h_\perp$ for $E_z = 0$. Constants H_0, g_e, and g_b are found numerically. The helicity-qubit operation regime in physical units is given in Table II, using both E_z and $h_\perp$ as external control parameters.

Qubit control.—A quantum coherent computation depends on the ability to control individual quantum degrees of freedom. Here we propose microwave MFGs for skyrmion qubit manipulation and gate operation. MFGs give rise to additional Hamiltonian terms $H_{ext}(t) = bf(t)\cos(\omega t + \phi_{ext})\cos\hat{\varphi}_0$, with $f(t)$ a dimensionless envelope function, or in terms of the qubit Hamiltonian, $H_{ext}^q = b_x(t)\hat{\sigma}_x$, with $b_x(t) = b_0 f(t)\cos(\omega t + \phi_{ext})$. In the diagonal basis, the driven Hamiltonian is written as

$$H_q = \frac{\omega_q}{2}\hat{\sigma}_z + b_x(t)[\cos\theta\hat{\sigma}_x + \sin\theta\hat{\sigma}_z], \quad (5)$$

with $\tan\theta = X_c/H_0$. To elucidate the role of the drive, we transform H_q into the rotating frame,

$$H_{rot} = \frac{\Delta\omega}{2}\hat{\sigma}_z + \frac{\Omega}{2}f(t)[\cos\phi_{ext}\hat{\sigma}_x + \sin\phi_{ext}\hat{\sigma}_y], \quad (6)$$

where $\Delta\omega = \omega_q - \omega$ is the detuning frequency and $\Omega = b_0\cos\theta$. Single-qubit operations correspond to rotations of the qubit state by a certain angle about a particular axis. As an example, for $\phi_{ext} = 0$ and $\Delta\omega = 0$, the unitary operator $U_x(t) = e^{-(i/2)\vartheta(t)\hat{\sigma}_x}$ corresponds to rotations around the x axis by an angle $\vartheta(t) = -\Omega\int_0^t f(t')dt'$ [38]. Rotations about the y axis are achieved for $\phi_{ext} = \pi/2$.

Qubit coupling scheme.—A key component for realizing a scalable quantum computer is an interaction Hamiltonian between individual qubits. As a straightforward scheme for

coupling skyrmion qubits, we consider the interlayer exchange interaction in a magnetic bilayer mediated by a nonmagnetic spacer layer (see Fig. 1 for a visualization). The interaction term is given by $F_{int} = J_{int}\int_{\mathbf{r}}\mathbf{m}_1\cdot\mathbf{m}_2$ [39], or in terms of the helicities, $H_{int} = -J_{int}\cos(\varphi_1 - \varphi_2)$. The resulting Hamiltonian in the qubit basis contains both transverse and longitudinal couplings,

$$H_{int} = -\mathcal{J}_{int}^x\hat{\sigma}_x^1\hat{\sigma}_x^2 - \mathcal{J}_{int}^z\hat{\sigma}_z^1\hat{\sigma}_z^2. \quad (7)$$

J_{int} can be tuned experimentally by changing the spacer thickness, while both $\mathcal{J}_{int}^{x,z}$ allow for an independent control by tuning all three external fields h, E_z, and $h_\perp$. This property is especially important in applications where both longitudinal and transverse couplings are desired, such as quantum annealing [38].

Noise and decoherence.—The interaction of the skyrmion qubit with the environmental degrees of freedom is a source of noise that leads to decoherence. They result in Ohmic damping terms for the collective coordinates φ_0 and S_z [40], accompanied by random fluctuating forces ξ_i that enter the quantum Hamiltonian as $\hat{H} \to \hat{H} + \xi_{\varphi_0}\hat{\varphi}_0 + \xi_{S_z}\hat{S}_z$. ξ_i is fully characterized by the classical ensemble averages $\langle\xi_i(t)\rangle = 0$ and $\langle\xi_i(t)\xi_j(t')\rangle = \delta_{ij}S_i(t-t')$ [34], and the correlator $S_i(t)$ is defined via the fluctuation-dissipation theorem, $S_i(\omega) = \alpha_i\omega\coth(\beta\omega/2)$, with α_i constants proportional to the Gilbert damping α. In terms of the reduced qubit Hamiltonian one finds

$$H_q = \frac{\omega_q}{2}\hat{\sigma}_z + \xi_x(t)\gamma_x\hat{\sigma}_x + \xi_y(t)\gamma_y\hat{\sigma}_y + \xi_z(t)\gamma_z\hat{\sigma}_z, \quad (8)$$

where γ_i constants which depend on the qubit type and $\xi_{x,y,z}$ are linear combinations of ξ_{φ_0} and ξ_{S_z}.

Within the Bloch-Redfield picture of two-level system dynamics, relaxation processes are characterized by the longitudinal relaxation rate $\Gamma_1 = T_1^{-1}$ and the dephasing rate $\Gamma_2 = T_2^{-1}$. The latter is a combination of effects of the depolarization Γ_1 and of the pure dephasing Γ_φ, combined to a rate $\Gamma_2 = \Gamma_1/2 + \Gamma_\varphi$, with $\Gamma_1 = \gamma_x^2 S_x(\omega_q) + \gamma_y^2 S_y(\omega_q)$ and $\Gamma_\varphi = \gamma_z^2 S_z(0)$ [41]. The optimal regime for realizing both long coherence and high anharmonicity is close to the degeneracy point and for $X_c \ll H_0$. This translates to the requirement $\bar{h} = 0.5$ and $E_z \ll 1$ for the S_z qubit, and to $\bar{h} = 1$ and E_z, $h_\perp \ll 1$ for the helicity qubit.

In Table II we present the expected qubit lifetimes for a modest choice of an ultralow Gilbert damping $\alpha = 10^{-5}$ and $T = 100$ mK. A skyrmion qubit has a moderately high coherence time in the microsecond regime. This is comparable to early measurements of the flux superconducting qubit and 2 orders of magnitude larger than the Cooper pair box [33]. The number of coherent Rabi frequency oscillations within the coherence time is $\Omega T_1 \propto 10^5$, inside the desired margins expected for superconducting qubits [34,42]. Several magnetic thin films exhibit ultralow Gilbert damping of the order of $\alpha \sim 10^{-4} - 10^{-5}$ [43–45]. In the sub-Kelvin qubit operational regime, Gilbert damping is expected to be even lower [46,47]. Coherence times can be further improved with the development of cleaner magnetic samples and interfaces in engineered architectures, without trading off qubit anharmonicity and scalability.

Readout techniques.—An essential part for implementing skyrmion-based quantum-computing architectures is a reliable readout. Quantum sensing of coherent single-magnon techniques, based on quantum dot [48] or superconducting qubit [49] sensors, is promising for the readout of S_z-qubit states, single magnetic excitations from the equilibrium configuration. On the other hand, helicity-qubit states represent two distinct skyrmion configurations with helicity values located at the two minima of the double-well potential of Eq. (4). Experimental observation of skyrmion helicity is possible using nitrogen-vacancy (NV) magnetometry [50], allowing for a detector-single qubit coupling control by varying the NV sensor distance from the skyrmion. Resonant elastic x-ray scattering [51] techniques provide a direct observation of skyrmion helicity, and when combined with ferromagnetic resonance measurements [52] can offer a promising single-qubit readout method. Finally, coupling a skyrmion to a magnetic force microscopy resonator allows the detection of magnetic states, which appear as resonance frequency shift signals [53].

Conclusions.—We proposed a novel physical qubit platform based on magnetic nanoskyrmions in frustrated magnets. The skyrmion state, energy-level spectra, transition frequency, and qubit lifetime are configurable and can be engineered by adjusting external electric and magnetic fields, offering a rich operation regime with high anharmonicity. Microwave pulses were shown to generate single-qubit gates for quantum computing, and skyrmion multiqubit schemes were considered for a scalable architecture with tailored couplings. Whereas, nonvolatile readout techniques can be employed for a reliable qubit state readout, using state-of-the-art magnetic sensing technology. We anticipate the considerable progress in the field of skyrmionics will provide exciting new directions on the development of skyrmion qubits as promising candidates for quantum computing technology.

*cpsaroud@caltech.edu
†christos@ntu.edu.sg

[1] T. D. Ladd, F. Jelezko, R. Laflamme, Y. Nakamura, C. Monroe, and J. L. O'Brien, Nature (London) **464**, 45 (2010).

[2] D. Loss and D. P. DiVincenzo, Phys. Rev. A **57**, 120 (1998).

[3] M. Grimm, A. Beckert, G. Aeppli, and M. Müller, PRX Quantum **2**, 010312 (2021).

[4] J. Preskill, Quantum **2**, 79 (2018).

[5] J. Clarke and F. K. Wilhelm, Nature (London) **453**, 1031 (2008).

[6] Y. Alexeev *et al.*, Phys. Rev. X Quantum **2**, 017001 (2021).

[7] A. N. Bogdanov and C. Panagopoulos, Nat. Rev. Phys. **2**, 492 (2020).

[8] T. Okubo, S. Chung, and H. Kawamura, Phys. Rev. Lett. **108**, 017206 (2012).

[9] A. O. Leonov and M. Mostovoy, Nat. Commun. **6**, 8275 (2015).

[10] S.-Z. Lin and S. Hayami, Phys. Rev. B **93**, 064430 (2016).

[11] X. Zhang, J. Xia, Y. Zhou, X. Liu, H. Zhang, and M. Ezawa, Nat. Commun. **8**, 1717 (2017).

[12] A. O. Leonov and M. Mostovoy, Nat. Commun. **8**, 14394 (2017).

[13] F. Matsukura, Y. Tokura, and H. Ohno, Nat. Nanotechnol. **10**, 209 (2015).

[14] X. Yao, J. Chen, and S. Dong, New J. Phys. **22**, 083032 (2020).

[15] A. Casiraghi, H. Corte-León, M. Vafaee, F. Garcia-Sanchez, G. Durin, M. Pasquale, G. Jakob, M. Kläui, and O. Kazakova, Commun. Phys. **2**, 145 (2019).

[16] C. Psaroudaki and D. Loss, Phys. Rev. Lett. **120**, 237203 (2018).

[17] Y. Okamura, F. Kagawa, M. Mochizuki, M. Kubota, S. Seki, S. Ishiwata, M. Kawasaki, Y. Onose, and Y. Tokura, Nat. Commun. **4**, 2391 (2013).

[18] P.-J. Hsu, A. Kubetzka, A. Finco, N. Romming, K. von Bergmann, and R. Wiesendanger, Nat. Nanotechnol. **12,** 123 (2017).

[19] R. Wiesendanger, Nat. Rev. Mater. **1,** 16044 (2016).

[20] V. Lohani, C. Hickey, J. Masell, and A. Rosch, Phys. Rev. X **9,** 041063 (2019).

[21] C. Psaroudaki, S. Hoffman, J. Klinovaja, and D. Loss, Phys. Rev. X **7,** 041045 (2017).

[22] M. H. Devoret, J. M. Martinis, and J. Clarke, Phys. Rev. Lett. **55,** 1908 (1985).

[23] J. M. Martinis, M. H. Devoret, and J. Clarke, Phys. Rev. Lett. **55,** 1543 (1985).

[24] D. D. Awschalom, J. F. Smyth, G. Grinstein, D. P. DiVincenzo, and D. Loss, Phys. Rev. Lett. **68,** 3092 (1992).

[25] L. Thomas, F. Lionti, R. Ballou, D. Gatteschi, R. Sessoli, and B. Barbara, Nature (London) **383,** 145 (1996).

[26] J. Brooke, T. F. Rosenbaum, and G. Aeppli, Nature (London) **413,** 610 (2001).

[27] C. Psaroudaki and D. Loss, Phys. Rev. Lett. **124,** 097202 (2020).

[28] T. Kurumaji, T. Nakajima, M. Hirschberger, A. Kikkawa, Y. Yamasaki, H. Sagayama, H. Nakao, Y. Taguchi, T.-h. Arima, and Y. Tokura, Science **365,** 914 (2019).

[29] J. L. Gervais and B. Sakita, Phys. Rev. D **11,** 2943 (1975).

[30] N. Dorey, J. Hughes, and M. P. Mattis, Phys. Rev. D **49,** 3598 (1994).

[31] See Supplemental Material at http://link.aps.org/supplemental/10.1103/PhysRevLett.127.067201 for information on the considered model, the skyrmion field quantization, the construction of basic qubit types, qubit control by microwave magnetic field protocols, and details on relaxation mechanisms.

[32] D. P. DiVincenzo, Fortschr. Phys. **48,** 771 (2000).

[33] M. Kjaergaard, M. E. Schwartz, J. Braumller, P. Krantz, J. I.-J. Wang, S. Gustavsson, and W. D. Oliver, Annu. Rev. Condens. Matter Phys. **11,** 369 (2020).

[34] S. Takei and M. Mohseni, Phys. Rev. B **97,** 064401 (2018).

[35] P. E. Roy, R. M. Otxoa, and C. Moutafis, Phys. Rev. B **99,** 094405 (2019).

[36] I. G. Arjana, I. Lima Fernandes, J. Chico, and S. Lounis, Sci. Rep. **10,** 14655 (2020).

[37] I. L. Fernandes, J. Chico, and S. Lounis, J. Phys. Condens. Matter **32,** 425802 (2020).

[38] P. Krantz, M. Kjaergaard, F. Yan, T. P. Orlando, S. Gustavsson, and W. D. Oliver, Appl. Phys. Rev. **6,** 021318 (2019).

[39] M. Poienar, F. Damay, C. Martin, J. Robert, and S. Petit, Phys. Rev. B **81,** 104411 (2010).

[40] O. A. Tretiakov, D. Clarke, G.-W. Chern, Y. B. Bazaliy, and O. Tchernyshyov, Phys. Rev. Lett. **100,** 127204 (2008).

[41] G. Ithier, E. Collin, P. Joyez, P. J. Meeson, D. Vion, D. Esteve, F. Chiarello, A. Shnirman, Y. Makhlin, J. Schriefl, and G. Schön, Phys. Rev. B **72,** 134519 (2005).

[42] M. H. Devoret and R. J. Schoelkopf, Science **339,** 1169 (2013).

[43] L. Soumah, N. Beaulieu, L. Qassym, C. Carrétéro, E. Jacquet, R. Lebourgeois, J. Ben Youssef, P. Bortolotti, V. Cros, and A. Anane, Nat. Commun. **9,** 3355 (2018).

[44] C. Guillemard, S. Petit-Watelot, L. Pasquier, D. Pierre, J. Ghanbaja, J.-C. Rojas-Sánchez, A. Bataille, J. Rault, P. Le Fèvre, F. Bertran, and S. Andrieu, Phys. Rev. Applied **11,** 064009 (2019).

[45] B. Heinrich, C. Burrowes, E. Montoya, B. Kardasz, E. Girt, Y.-Y. Song, Y. Sun, and M. Wu, Phys. Rev. Lett. **107,** 066604 (2011).

[46] H. Maier-Flaig, S. Klingler, C. Dubs, O. Surzhenko, R. Gross, M. Weiler, H. Huebl, and S. T. B. Goennenwein, Phys. Rev. B **95,** 214423 (2017).

[47] A. Okada, S. He, B. Gu, S. Kanai, A. Soumyanarayanan, S. T. Lim, M. Tran, M. Mori, S. Maekawa, F. Matsukura, H. Ohno, and C. Panagopoulos, Proc. Natl. Acad. Sci. U.S.A. **114,** 3815 (2017).

[48] D. M. Jackson, D. A. Gangloff, J. H. Bodey, L. Zaporski, C. Bachorz, E. Clarke, M. Hugues, C. Le Gall, and M. Atatüre, Nat. Phys. **17** (2021), 585.

[49] D. Lachance-Quirion, S. P. Wolski, Y. Tabuchi, S. Kono, K. Usami, and Y. Nakamura, Science **367,** 425 (2020).

[50] Y. Dovzhenko, F. Casola, S. Schlotter, T. X. Zhou, F. Büttner, R. L. Walsworth, G. S. D. Beach, and A. Yacoby, Nat. Commun. **9,** 2712 (2018).

[51] S. L. Zhang, G. van der Laan, W. W. Wang, A. A. Haghighirad, and T. Hesjedal, Phys. Rev. Lett. **120,** 227202 (2018).

[52] S. Pöllath, A. Aqeel, A. Bauer, C. Luo, H. Ryll, F. Radu, C. Pfleiderer, G. Woltersdorf, and C. H. Back, Phys. Rev. Lett. **123,** 167201 (2019).

[53] E. Marchiori, L. Ceccarelli, N. Rossi, L. Lorenzelli, C. L. Degen, and M. Poggio, arXiv:2103.10382.

Skyrmion Qubits:
Challenges For Future Quantum Computing Applications

Christina Psaroudaki,[1] Elias Peraticos,[2] and Christos Panagopoulos[2]

[1)]*Laboratoire de Physique de l'École normale supérieure, ENS, Université PSL, CNRS, Sorbonne Université, Université de Paris, F-75005 Paris, France*

[2)]*Division of Physics and Applied Physics, School of Physical and Mathematical Sciences, Nanyang Technological University, 21 Nanyang Link 637371, Singapore*

(*Electronic mail: christos@ntu.edu.sg)

(*Electronic mail: christina.psaroudaki@phys.ens.fr)

(Dated: 9 January 2024)

Magnetic nano-skyrmions develop quantized helicity excitations, and the quantum tunneling between nano-skyrmions possessing distinct helicities is indicative of the quantum nature of these particles. Experimental methods capable of non-destructively resolving the quantum aspects of topological spin textures, their local dynamical response, and their functionality now promise practical device architectures for quantum operations. With abilities to measure, engineer, and control matter at the atomic level, nano-skyrmions present opportunities to translate ideas into solid-state technologies. Proof-of-concept devices will offer electrical control over the helicity, opening a promising new pathway towards functionalizing collective spin states for the realization of a quantum computer based on skyrmions. This Perspective aims to discuss developments and challenges in this new research avenue in quantum magnetism and quantum information.

Authors to whom correspondence should be addressed: Christina Psaroudaki, christina.psaroudaki@phys.ens.fr; Christos Panagopoulos, christos@ntu.edu.sg

I. INTRODUCTION

Quantum computers have the potential to revolutionize data storage and processing beyond their conventional counterparts[1], making it a prominent area of research. Although quantum computers hold great promise, their realization and the identification of practical applications pose several challenges[2]. Research and development of new qubit technologies are therefore pursued intensely across different solid-state platforms. Among them, topological spin textures, such as magnetic skyrmions, are emerging as promising macroscopic qubits[3] due to their topological stability and nanosize. These topological excitations with particle-like behavior are highly resilient to external perturbations[4,5] and have primarily been exploited for a wide range of classical applications, ranging from spintronics devices[4,6] to unconventional computation platforms[7,8].

The observation of nanometer-scale skyrmions[9–11] along with their stability in the milli-Kelvin regime, inspired an increasing number of studies on their quantum properties[12–27], expanding their potential for information processing from the classical to the quantum regime. These developments create the possibility of utilizing the quantum dynamics of magnetic skyrmions and bridge the skyrmionics field to quantum information, analogously to the highly interdisciplinary field of quantum magnonics[28]. At the same time, the advancement of sensors capable of detecting magnetic signals with quantum sensitivity[29,30] and the discovery of novel skyrmion hosting materials[10,11] make the investigation of the quantum aspects of magnetic skyrmions experimentally feasible.

Harnessing quantum functionalities requires identifying systems with discrete energy levels while satisfying several criteria, including scalability, controllability, and readout by nonvolatile techniques[31]. Skyrmion qubits use the energy-level quantization of skyrmion helicity to encode quantum information[3]. Thus, in contrast to other platforms based on natural microscopic systems, skyrmion qubits are built upon macroscopic collective variables, similar in nature to superconducting quantum circuits[32,166]. The applicability of the classical variable of helicity to quantum operations depends on the feasibility of quantum tunneling between two macroscopic states with distinct helicities. For a nanoskyrmion that is sufficiently decoupled from its environment, tunable macroscopic quantum tunneling has been predicted to occur within experimental reach[33].

Centrosymmetric materials are a prominent platform for constructing skyrmion quantum processors[3]. In this class of materials, geometrical frustration renders the skyrmion helicity a quantum degree of freedom and leads to a higher density of skyrmions[167]. Here, skyrmions are considerably smaller[5] than those in non-centrosymmetric magnets. Skyrmion lattice phases have already been observed in gadolinium compounds and perovskite oxides[5]. Whereas new materials are expected to emerge as the field of frustrated magnetism progresses[35].

Skyrmion qubits inherit the appealing physical properties of classical magnetic skyrmions, allowing for compact, high-density, and low-energy devices. Their size, positional stability, lifetime, and energetics can be tuned by material engineering and geometrical control[36]. Their precise nucleation, detection, and dynamics have been extensively explored using a wide range of experimental methods[37]. Furthermore, the low energy-level spectra of skyrmion qubits are configurable by external magnetic and electric fields and can be designed to exhibit the desired qubit properties, including operation regimes, transition frequencies, anharmonicity, and qubit lifetime. Microwaves can be utilized for qubit manipulation and gate operation, while nonvolatile measurement schemes
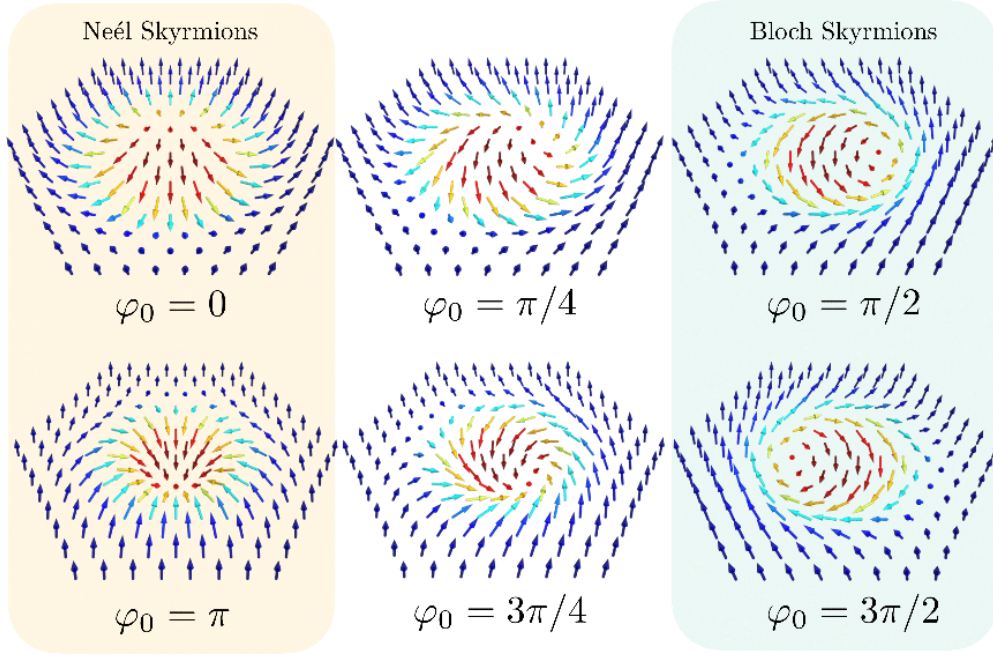
FIG. 1. Illustrations of a series of 2D skyrmion textures with topological charge $Q = 1$ and different helicities φ_0. The arrows denote the spin direction and the out-of-plane spin component is represented by color. Neél (left panel) and Bloch (right panel) are stabilized in DMI systems, while in frustrated magnets all possible configurations are allowed, separated by small energy gaps generated by additional anisotropies or dipolar interactions.

can be employed for a reliable qubit state readout. Scalability is addressed by tailored coupling schemes between individual qubits.

Despite the potential for competitive technology, the development of a skyrmion quantum processor will face near-term challenges. On a fundamental level, these include among others the identification of candidate frustrated magnets with low damping, the microscopic understanding and control of noise sources, the design of optimal gate implementations, longer qubit coherence times, and tunable coupling of spatially separated qubits. On a device-specific level, the deterministic and precise skyrmion nucleation, the efficient determination of the fidelity of quantum operations, and robust and reproducible device fabrication are among the pressing issues to be addressed.

The purpose of this Perspective is to present the quantum aspects of magnetic skyrmions and their usage in quantum operations and to discuss challenges and future directions in achieving skyrmion-based quantum technology. The main advantage lies in the high degree of control in skyrmion manipulation, qubit parameter tunability, and all-magnetic device integration. Whilst technical challenges would need to be overcome first, the application of skyrmions in the quantum regime is expected to lead to disruptive technologies, opening up new research opportunities in the fields of skyrmionics and quantum magnetism.

II. QUANTUM PROPERTIES OF MAGNETIC SKYRMIONS

Magnetic skyrmions emerge as topologically nontrivial configurations of the magnetization field $\mathbf{m}(\mathbf{r}, t)$ in certain helimagnetic materials[5], characterized by a finite topological charge $Q = 1/4\pi \int d\mathbf{r}\mathbf{m} \cdot (\partial_x \mathbf{m} \times \partial_y \mathbf{m})$[38]. They have been discovered in a plethora of magnetic bulk crystals[5] and multilayers[39] and extensively investigated theoretically and experimentally[37].

Figure 1 shows a schematic of a series of single skyrmion configurations in two dimensions (2D). They are characterized by $\Phi = \mu\phi + \varphi_0$ and $\Theta = \Theta(\rho)$ with boundary conditions $\Theta(0) = \pi$ and $\Theta(\infty) = 0$, where $\{\rho, \phi\}$ are the polar coordinates, and $\mathbf{m} = [\sin\Theta\cos\Phi, \sin\Theta\sin\Phi, \cos\Theta]$ is the normalized magnetization. Here φ_0 denotes the skyrmion helicity and corresponds to the angle of the global rotation around the z-axis, while μ corresponds to the skyrmion vorticity and defines the topological charge, $Q = \mu$, for fixed boundary conditions. Due to the macroscopic size of magnetic skyrmions, their dynamics are typically governed by the purely classical Landau-Lifshitz-Gilbert (LLG) equation[40]. The long-time dynamics of skyrmions reduce to a much simpler problem by considering generalized collective coordinates with long relaxation times[41]. They describe the overall movement of the magnetic texture and are associated with a continuous symmetry broken by the skyrmion configuration.

For skyrmions at the nanometer scale and at temperatures much lower than the ordering transition, these degrees of freedom are expected to be affected by quantum fluctuations and
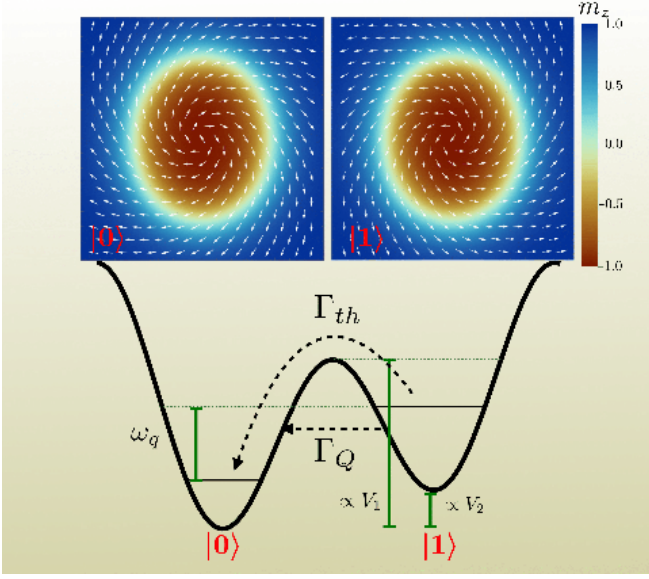
FIG. 2. Representation of skyrmion helicity potential landscape. The logic space $|0\rangle$ and $|1\rangle$ is consisted of two macroscopic states with distinct helicities, localized at the two potential minima, separated by a tunable energy barrier. In the absence of bias V_2, macroscopic quantum tunneling through the barrier hybridizes the degenerate levels and introduces a level splitting.

are promoted to quantum mechanical operators[42]. Their dynamics resemble quantum mechanical particles, which exhibit quantum tunneling between classically stable magnetic configurations, a necessary property to device elements of quantum computers[43]. The skyrmion center operator $\hat{\mathbf{R}}$ satisfies the commutation relation $[\hat{R}_x, \hat{R}_y] = ia^2/4\pi SQ$, with a the lattice constant and S the spin magnitude. Here the magnetic length $\ell = a/\sqrt{4\pi S|Q|}$ measures the extension of quantum fluctuations in the phase space of collective coordinates[42]. In the classical limit of large $S \to \infty$, it holds $\ell \gg a$, and quantum effects become weak. The quantum treatment of the skyrmion propagation in chiral magnetic insulators revealed that observable quantum behavior may arise for $\hat{\mathbf{R}}$ in the presence of pinning defects that split the lowest Landau level into quantized levels[15]. In addition, the quantum fluctuations around the skyrmionic configuration give rise to a quantum mass term $\mathscr{M}$ with an explicit temperature dependence which remains finite even at a vanishingly small temperature[12]. For sufficiently small skyrmions, a quantum liquid phase appears as an intermediate phase between the skyrmion crystal and the ferromagnet[13].

Evidence of quantum behavior in magnetic systems stems from the prediction and observation of macroscopic quantum tunneling events[44–48]. The quantum tunneling probability Γ_Q is governed by the zero-temperature WKB exponent, $\Gamma_Q \propto e^{-S_0}$, with S_0 temperature-independent. Above a critical temperature $T_c \approx \hbar U_0/k_B S_0$, with U_0 the tunneling barrier, classical thermal events with $\Gamma_{th} \propto e^{-U_0/T}$ dominate over the quantum tunneling-induced transitions[49] (see Fig. 2 for a schematic illustration). The quantum depinning of the skyrmion position out of an impurity potential suggests that

sufficiently small magnetic skyrmions will behave as quantum objects with T_c in the millikelvin temperature regime and Γ_Q^{-1} within a few seconds[20]. The problem resembles quantum depinning in the Hall-type dynamics of a vortex in high-T_c superconductors[50] or a charged spin texture in quantum Hall systems[51], and describes the quantum behavior observed in similar mesoscopic particles[48,52]. The quantum collapse of a classically stable skyrmion has been predicted to occur through under-barrier quantum tunneling to the ferromagnetic state[19], with T_c estimated to be a few Kelvin for realistic material parameters[21]. In the opposite scenario, single skyrmions are quantum mechanically nucleated from the ferromagnetic state in the presence of local magnetic fields[22].

In addition to the usual translational modes $\mathbf{R}$, a skyrmion stabilized in a model with an unbroken rotational symmetry possesses the skyrmion helicity φ_0 as an extra degree of freedom. Following the method of collective coordinate quantization, φ_0 and its conjugate momentum associated with global spin rotations $S_z = \int d\mathbf{r}(1 - \cos\Theta)\partial_\phi\Phi$ are promoted to quantum operators satisfying $[\hat{\varphi}_0, \hat{S}_z] = i/S$ with the classical limit recovered when $S \to \infty$[3]. Potential engineering achieved by introducing external perturbations for the skyrmion helicity allows the observation of diverse macroscopic quantum phenomena. For sufficiently small skyrmions with radius $\lambda \approx 5 - 10$ nm and a modest choice of effective spin $S \approx 1 - 10$, quantum tunneling processes between two macroscopic states with distinct helicities occur with Γ_Q^{-1} within seconds below 100 mK. Macroscopic quantum coherence between degenerate states causes MHz-level energy tunnel splitting while tunneling in periodic potentials results in destructive quantum interference among equivalent tunneling paths[33]. Hence, quantum tunneling, a fundamental aspect of quantum computing, is expected to be common and experimentally feasible in magnetic nano-skyrmions.

III.   SKYRMION QUANTUM COMPUTING

Magnetic skyrmions are particularly promising candidates for information processing and computing due to their single-particle properties. In conventional logic devices, logic numbers 0 and 1 are associated with the presence or absence of magnetic skyrmions in racetrack devices[53,54]. Their physical properties, including nano-size, parameter tunability, and low-energy operation, render them potential candidates for unconventional computing approaches such as neuromorphic[8,55], reservoir[56] and probabilistic[7]. As discussed earlier, although magnetic skyrmions are macroscopic in size, under appropriate conditions they display generic quantum properties such as quantized energy levels, superposition of states, entanglement, and quantum tunneling. Thus, they offer a new class of primitive building blocks for quantum computers, extending their suitability from the classical to the quantum regime.

A. Skyrmion Qubits

Skyrmions can be generated in magnetic systems through various mechanisms, often acting simultaneously. In systems that lack inversion symmetry, the relativistic DMI energetically stabilizes skyrmions[57], with uniquely defined $\mu = \pm 1$ and a potential term $\sin(\varphi_0)$ (Bloch skyrmions) or $\cos(\varphi_0)$ (Néel skyrmions) depending on the DMI form, which in turn is determined by the crystal symmetry of the material (see Fig. 1 for a schematic illustration). The DMI strength controls the skyrmion size, which typically ranges between 10-100 nm. Long-ranged magnetic dipolar interactions generate skyrmions of the order of 100 nm-1 μm with two degenerate lowest-energy states $\varphi_0 = \pm\pi/2$[58]. Frustrated exchange interactions[59] and four-spin exchange interactions[9] support atomic-sized skyrmion structures, and helicity can take any arbitrary value. Hence, magnetic frustration offers advantages for quantum information processing based on skyrmions because i) it provides a path to scale down the skyrmion size, a prerequisite for quantum effects to be strong and ii) skyrmion helicity is a zero mode and does not experience large potential terms. Importantly, helicity couples effectively to external perturbations, and the system can be driven to the optimum quantum regime[33].

A skyrmion qubit is constructed based on the energy-level quantization of the helicity degree of freedom of a skyrmion stabilized in a 2D nanodisk. The reduced dynamics of the system are given in terms of the quantum Hamiltonian $H = \hat{S}_z^2/2\mathcal{M} + h_1\hat{S}_z + V(\hat{\varphi}_0)$, where $\mathcal{M}$ is the mass for the skyrmion helicity, h_1 is the Zeeman term under the application of a uniform magnetic field, while the helicity potential can be written in its most general form as $V(\hat{\varphi}_0) = V_0\cos 2\hat{\varphi}_0 - V_1\cos\hat{\varphi}_0 + V_2\sin\hat{\varphi}_0$. The first term can be the result of dipole-dipole interaction[60], in-plane uniaxial[61], or in-plane four-fold crystal anisotropy[62]. In the absence of intrinsic anisotropy, a piezoelectric stressor[63] or the lattice mismatch between the magnetic layer and the nonmagnetic substrate[64,65] can induce anisotropy constants with a wide range of tunability. The application of an electric field produces the second term and provides a direct external parameter to tune skyrmion helicity[66], while the last term corresponds to the application of an external magnetic field gradient or the presence of a DMI term.

Depending on the parameter regime, two fundamental qubit designs are identified based on eigenstates of either $\hat{S}_z$, quantized magnetic excitations of the perpendicular to the 2D plane magnetization component, or $\hat{\varphi}_0$ states with a well-defined helicity. Notably, the former type resembles the superconducting charge qubit based on the number of Cooper pairs, while the latter the flux qubit based on quantized magnetic flux in a superconducting loop[67]. The eigenstates of both qubit designs are mapped on a simple physical basis and are therefore useful for quantum annealing[68]. Analogous to the anharmonicity caused by the nonlinear inductance of superconducting Josephson junctions, the electric field produces the necessary nonlinearity, causing non-equidistant level spacing.

Indeed, the operation of the skyrmion qubit relies heavily on the anharmonicity of the well potential, in order to individually address transitions between quantized levels with a distinct frequency. By tuning the external electric and magnetic fields, a relatively large anharmonicity can be achieved $|\omega_{ex} - \omega_q| > 20\%\omega_q$, where ω_q is the qubit frequency and ω_{ex} the frequency of higher level transitions[3]. This implies, that although the qubit frequencies between neighboring qubits depend on the fabrication process precision, the system will not suffer from the frequency collisions expected in weakly anharmonic multi-qubit systems[69].

The lowest two states $|0\rangle$ and $|1\rangle$ of the skyrmion Hamiltonian H span the computational space and naturally form a tight two-level system with an approximate Hamiltonian

$$H_q = \frac{H_0}{2}\hat{\sigma}_z - \frac{X_c}{2}\hat{\sigma}_x, \tag{1}$$

where the form of H_0 is given in terms of the original parameters and depends on the qubit design, and X_c is the control parameter that corresponds to either the electric field or the magnetic field gradient. In Eq. (1), $\hat{\sigma}_{z,x}$ refer to the Pauli spin operators. The qubit frequency is $\omega_q = \sqrt{H_0^2 + X_c^2}$. Helicity qubits work close to the degeneracy point $h_1 S\mathcal{M} = -1$, where the helicity degree of freedom becomes dominant and can be considered as the discrete variable. In the limit of large potential strengths $V_i \gg 1$, the lowest two states are well described by symmetric and antisymmetric combinations of the two wave functions localized in each well (see Fig. 2 for a representation). The qubit can be in a superposition of these two macroscopic states with distinct helicities, a manifestation of the quantum mechanical behavior of a macroscopic system. Coherent tunneling between these degenerate states through the potential barrier lifts the degeneracy and results in an energy-splitting of the order of MHz, well decoupled from the spectrum of higher levels in the GHz regime.

B. Noise and Decoherence

Skyrmion qubits are macroscopic in size and are expected to be sensitive to environmental noise. The interaction with uncontrolled degrees of freedom, both extrinsic and intrinsic, inevitably results in quantum decoherence, a key challenge to address in the practical development of qubit devices. It is a delicate matter to isolate the qubit from a perturbing environment, and desirable operation and unwanted perturbation (noise) go hand in hand. Important timescales for the qubit decoherence are the energy relaxation time T_1 and dephasing time T_2. The former quantifies the decay of the first excited state $|1\rangle$ to the ground state $|0\rangle$, while the latter corresponds to the time over which the phase difference between two eigenstates in a quantum superposition state becomes randomized. Both T_1 and T_2 are important to estimate the expected accuracy of quantum operations and can be evaluated by a weak coupling of the skyrmion qubit to the quantum environmental noise.

Decoherence times are estimated starting from the magnetization dynamics encoded in the Landau-Lifshitz-Gilbert equation (LLG)[70,71]. Possible damping mechanisms for the collective coordinate of helicity are parameterized by a phenomenological velocity-dependent Ohmic term $\alpha_{\varphi_0}\dot{\varphi}_0$ induced by
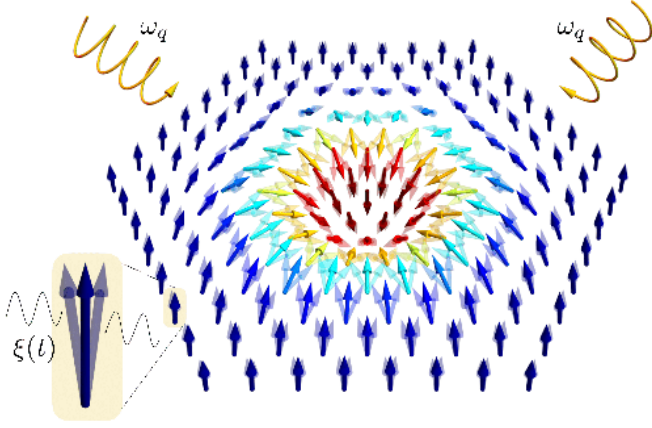
FIG. 3. A magnetic skyrmion in the presence of noise gives rise to random fluctuating forces $\xi(t)$ (black arrows) acting on the skyrmion qubit, leading to decoherence. Driving the system with microwave magnetic fields (yellow arrows) at the qubit transition frequency ω_q can be used for single-qubit operations.

the coupling of the skyrmion to other unspecified degrees of freedom[3]. Here α_{φ_0} is a constant proportional to the Gilbert damping α. Dissipation terms are accompanied by random fluctuating forces ξ_i, entering the quantum Hamiltonian as $H_q = -\frac{1}{2}\omega_q \sigma_z + \xi_\perp \sigma_\perp + \xi_z \sigma_z$, where $\sigma_\perp$ denotes the transverse spin components $\sigma_{x,y}$ (see Fig. 3 for a visualization). Noise sources are conveniently described by their quantum spectral density $\langle \xi_i(t)\xi_j(t')\rangle = \delta_{ij}S_{ij}(t-t')$, linked to the dissipative terms via the fluctuation-dissipation theorem. Using the standard Bloch-Redfield[72,73] picture of two-level system dynamics, both T_1 and T_2 are estimated to be in the microsecond regime, thus comparable to early measurements of the flux superconducting qubit and two orders of magnitude larger than the Cooper pair box[74]. Here we assume an ultra-low Gilbert damping $\alpha = 10^{-5}$ and low operational temperature $T = 100$ mK.

Although the total noise experienced by the skyrmion has multiple origins, the phenomenological LLG equation leaves the microscopic details of the skyrmion-environment coupling unspecified. Decoherence rates can be estimated more precisely by deriving a microscopic description of the properties of skyrmions coupled to quasiparticles naturally excited due to thermodynamics, i.e. itinerant electrons, phonons, and magnons. In magnetic insulators and at low enough temperatures, the spin degrees of freedom are the prominent source of noise. A microscopic treatment of the dynamics of the skyrmion center-of-mass coupled with a bath of magnon-like quantum excitations predicts super-Ohmic damping terms at temperatures below the magnon gap, which remain finite down to zero temperature due to the quantum nature of the bath[12]. Damping terms are accompanied by random stochastic fields with a colored auto-correlation function[75] and have a less detrimental effect on the quantum behavior of mesoscopic systems when compared with Ohmic-like noises with short correlation times[76,77].

In metallic ferromagnets, conduction electrons have strong

effects on the skyrmion motion, as they generate (non)-adiabatic spin-transfer torques and damping terms[78]. Within a field-theoretical treatment, the non-adiabatic contribution of conduction electrons gives rise to quantum inertia terms calculated microscopically[79–81]. Finally, an inertia mass has been computed exactly as the result of the skyrmion-phonon interaction within a toy model of the magnetoelastic coupling[82]. Generalization of the above theoretical approaches to include the coupling of the skyrmion helicity φ_0 to quasiparticle noise sources is straightforward and will result in a more accurate estimation of the decoherence times.

Other types of noise include local fluctuating electric and magnetic fields, nuclear spins and dipolar interactions, structural defects in the sample and at interfaces, contributions from the leads connected to the solid-state devices, as well as systematic noise associated with the microwave pulse resonator or readout circuits. The degree to which a qubit is influenced by these noise sources is related to the qubit's susceptibility, which in turn is determined by fabrication processes, cryogenic engineering, and electronics design. Longer coherence times can be achieved by developing a design strategy aiming to operate at the skyrmion qubit's optimal regime.

C. Universal Quantum Computing

Quantum algorithms are implemented by a small set of single-qubit and two-qubit unitary operations, the basis of the future skyrmion quantum processors. Single-qubit gates $U_i(\theta)$ rotate an arbitrary Bloch vector at a certain angle θ about a particular axis $i = \{x,y,z\}$, while two-qubit entangling operations are generally conditional gates involving two qubits. A complete single-qubit gate set supplemented with an entangling two-qubit operation suffices for universality, in the sense that all unitary operations on arbitrarily many bits can be expressed as compositions of these gates[83]. A common universal quantum gate set is $\mathscr{G}_0 = \{U_x(\theta), U_y(\theta), U_z(\theta), U_{\text{ph}}(\theta), U_{\text{CNOT}}\}$, where $U_{\text{ph}}(\theta) = e^{i\theta}\mathbb{1}$ applies a phase θ and U_{CNOT} flips the state of the second qubit conditioned on the first qubit being in state $|1\rangle$. Another universal gate set is $\mathscr{G}_1 = \{U_H, U_S, U_T, U_{\text{CNOT}}\}$, where the U_H Hadamard gate performs a π rotation about the $(x+z)/2$ axis, and the U_S (U_T) rotates the qubit state by $\pi/2$ ($\pi/4$) around the z axis. Any other single-qubit gate can be approximated using only single-qubit gates from $\mathscr{G}_1$[84].

1. Single-Qubit Gates

Microwave magnetic field gradients with frequencies at the qubit transition ω_q can be used to drive single-qubit gates[3]. In particular, one can generate rotations around the x and y axis by controlling the coupling between the qubit states $|0\rangle$ and $|1\rangle$ using microwave pulses. The driven qubit Hamiltonian in the frame rotating with the qubit frequency reads $H_q = \Delta\omega_q/2\sigma_z + \Omega f(t)/2[\cos\phi\,\sigma_x + \sin\phi\,\sigma_y]$, where $\Delta\omega = \omega_q - \omega$ is the detuning frequency with ω the frequency of the microwave source, Ω depends on the external field amplitude,

$f(t)$ is a dimensionless pulse-envelope function and ϕ the phase of the external drive. Rotation around the x axis by an angle $\vartheta(t) = -\Omega \int_0^t f(t')dt'$, i.e. $U_x(\vartheta(t)) = e^{-i\vartheta(t)\sigma_x}$, is performed using resonant driving $\omega = \omega_q$ and in-phase pulses $\phi = 0$. Analogously, $U_y(\vartheta(t))$ is achieved with out-of-phase pulses $\phi = \pi/2$.

Rotations around the remaining z axis are generated by adjusting the phase ϕ of the drive. These are known as virtual zero-duration U_z gates and correspond to adding a phase offset to the drive field for subsequent U_x and U_y gates[85]. In addition to microwave gates, a time-dependent electric field protocol generates the $U_z(\theta)$ gate, while a time-dependent spin current performs rotations of the Bloch vector around the x axis and generates the $U_x(\theta)$ gate[86]. It becomes apparent that the gates $U_{x,y,z}$ are simple to implement and are natively available in a skyrmion quantum processor. Any SU(2) gate is constructed by combining U_z and U_x gates[85]. As an example, the Hadamard gate is expressed as $U_H = U_z(\pi/2) \cdot U_x(\pi/2) \cdot U_z(\pi/2)$.

2. Two-Qubit Gates

Alongside arbitrary single-qubit gates, the universality of particular quantum hardware is demonstrated by outlining methods for generating two-qubit gates. Among them, the controlled-NOT (CNOT) gate and the controlled phase (CZ) are commonly used points of reference in the creation of quantum circuits. CNOT flips the state of the target qubit and CZ applies a Z gate to the target qubit, conditioned on the control qubit being in state $|1\rangle$.

In magnetic materials, the interlayer exchange interaction provides a straightforward two-skyrmion coupling scheme[3]. Bilayers inherently give rise to interacting skyrmions across various interfaces with distinct helicity-dependent dynamical phenomena[87,88]. The ferromagnetic interaction term $-J_{\text{int}} \int_{\mathbf{r}} \mathbf{m}_1(\mathbf{r}) \cdot \mathbf{m}_2(\mathbf{r})$, with $i = \{1,2\}$ the layer index, translates into interaction between the two skyrmion helici-
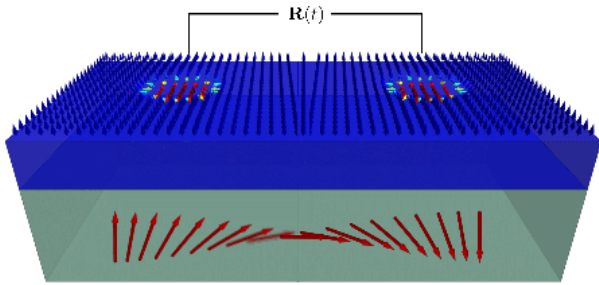

FIG. 4. Illustration of a two-skyrmion coupling scheme. Two magnetic skyrmions corresponding to two distinct qubits are placed in a nanowire (blue), separated by a distance $\mathbf{R}(t)$. Two-qubit gates are implemented by a time-dependent external field protocol controlling $\mathbf{R}(t)$. Alternatively, long-distance two-qubit entanglement is possible via magnon modes (red arrows) excited in low-damping magnetic materials (green).

ties $H_{\text{int}} = -J'_{\text{int}} \cos(\varphi_1 - \varphi_2)$ and a two-qubit Hamiltonian with both transverse and longitudinal couplings, $H_{\text{int}} = -\mathscr{J}^x_{\text{int}} \sigma^1_\perp \sigma^2_\perp - \mathscr{J}^z_{\text{int}} \sigma^z_1 \sigma^z_2$. The interlayer interaction J_{int} is controlled by either a nonmagnetic insulating spacer, such that J_{int} decays exponentially with the spacer thickness, or a metallic spacer, such that the exchange interaction oscillates and can change sign[87]. Alternatively, J_{int} is tuned by varying the distance between the layers.

The two-qubit Ising interaction $\mathscr{J}^z_{\text{int}} \sigma^z_1 \sigma^z_2$ yields the CNOT and CZ gates directly using one two-bit operation[89] under a time-dependent skyrmion bilayer interaction protocol[86]. The two skyrmion-qubit Heisenberg interaction $\mathscr{J}_{\text{int}}(\sigma^x_1 \sigma^x_2 + \sigma^y_1 \sigma^y_2 + \sigma^z_1 \sigma^z_2)$ corresponds to the SWAP operation that exchanges the states of two qubits[89] and can generate the CNOT gate by two two-bit operations[89]. Two-qubit gates in magnetic domain wall qubits are implemented using the coupled dynamics of the DW position and chirality[90], similar to the coupling of the skyrmion helicity to the translational motion[60].

In addition to the direct bilayer magnetic interaction, spatially separated skyrmion qubits can be entangled using their interaction to delocalized degrees of freedom. Quasiparticle-mediated entanglement proposals for hybrid quantum systems provide a high degree of control over interactions between solid-state magnetic qubits. Long-distance spin-qubit coupling via magnon modes in ferromagnets can be achieved under realistic experimental conditions[91] (see Fig. 4 for a visualization of the entanglement platform). Photon-mediated magnon-magnon coupling between magnetoelectrically active skyrmion excitations in a cavity can be used to generate entanglement between magnon qubits[92]. These schemes are directly extended to the skyrmion qubit platform and allow the design of optimal protocols for gate synthesis[93].

D. Qubit Readout

Quantum computing requires coupling quantum systems to external instruments for control and readout. We need fast and accurate qubit readout and hardware that facilitates high qubit connectivity. The challenge, however, is to control and measure qubits while prohibiting unwanted interactions with their environment and scaling them up to larger systems. One architecture for realizing quantum processors can be skyrmion qubits coupled to coplanar waveguide resonators for readout and control of one another. The resonator frequency is qubit-state dependent, and thus, through probing this resonator, it becomes possible to discern the qubit state. Applying a readout tone at the qubit frequency, we can measure the state-dependent phase shift of the reflected readout tone. Detectors with a few electrodes, high readout fidelity, and speed are required to discern the skyrmion qubit state in a measurement time of under a few microseconds. In other words, a timescale shorter than the decoherence time, $T_{1,2}$, enables the implementation of error correction.

Before devices are developed, however, it is important to demonstrate experimentally the quantization of helicity. Helicity-qubit states represent two distinct skyrmion configurations with helicity values located at the two minima of

the double-well potential[3]. Microwave techniques are especially suitable to characterize materials exhibiting non-collinear textures. Resonant modes detecting helicity shifts can be traced as a function of frequency, magnetic, and electric fields. Resonance probes can detect eigenstate transitions in individual skyrmions, either by magnetic resonance force microscopy (MRFM)[94,95], or by using a magnetic force microscopy (MFM) tip as a local microwave probe[94–99].

Ferromagnetic Resonance (FMR) is a useful method to distinguish helicities, and detect gyration and breathing modes of skyrmions[98,99], with a quantized level shift manifesting as a discontinuity in the resonance frequency in the millikelvin regime. For a skyrmion radius of only a few nanometers, it is challenging to probe single skyrmions, and therefore collective excitations need to be analyzed in a magnetically homogeneous material. A complementary approach is circular X-ray polarization combined with a microwave drive to track Rabi oscillations. Furthermore, single nitrogen-vacancy in diamond tips has been shown to detect skyrmion helicities[100,101], although a spatial resolution of less than 10 nm remains a challenge[102–105]. At a practical level, spin helicity in itinerant non-collinear magnets can be controlled with the use of magnetic fields and electric currents. Hence, a convenient read out is possible by second-harmonic resistivity, and via tunneling magnetoresistance at a segment of the skyrmion, potentially enabled by advances in nanofabrication capabilities[106,107].

IV. FUTURE PERSPECTIVES

Finding and stabilizing new spin configurations in materials is one of the fundamental goals of condensed matter physics. A plethora of compounds exhibit a remarkable range of magnetic phases including nano-skyrmions that are of direct relevance to quantum technology. While the traditional approach has been to search for such phases within naturally occurring compounds, advances in the angstrom-scale layer-by-layer synthesis of multi-element compounds for materials by design have taken the approach to a new level of power and sophistication. This grants access to a controlled terrain of materials engineering and electronic operations at the atomic scale, a particularly appealing hunting ground for new physics and targeted applications. Already, the potential of certain nano-skyrmions for quantum hardware has triggered proposals for device and circuit configurations. Combined with the availability of materials hosting nano-skyrmions with distinct helicity, this engenders fundamentally new helicity-based operations in a convenient parameter space, with much promise for a skyrmion-based qubit.

A. Candidate Materials

Candidate materials for a skyrmion qubit architecture need to satisfy certain criteria. A variable-helicity skyrmion qubit may be materialized in frustrated magnets with a suitable crystal structure and ultra-low Gilbert damping of 10^{-5} to 10^{-4}. Insulating materials are preferable for placing electronic gates

in direct contact with the magnetic film, but so far are rare hosts of sub-10 nm skyrmions at low temperatures. On the other hand, there is already encouraging evidence in metallic frustrated magnets with low and tunable charge carrier density. Here, an insulating layer placed between the gates and the magnet would allow the desired nonvolatile control.

Promising candidates include $Gd_3Ru_4Al_2$ and Gd_2PdSi_3[10,11,108]. Gd_2PdSi_3 features frustrated triangular lattice planes of magnetic Gd ions interleaved with a non-magnetic $PdSi_3$ honeycomb lattice. Other rare earth intermetallic magnets share the same space group, including RGa_2 (where R is a rare earth element) and $ErSi_2$[110,111]. The weak ferromagnet $TbGa_2$[112] shows signatures indicative of a non-collinear magnetic ground state[10,11,113]. $NiGa_2S_4$ is a Mott insulator built on a triangular lattice[114–116], with a non-collinear antiferromagnetic ground state[115,117].

α-$NaFeO_2$ is also potentially promising although it is not yet clear whether its short-range spin correlations support a skyrmion lattice[113]. Bloch-type skyrmionic bubbles with degenerate $\pi/2$ and $-\pi/2$ helicities have been reported to stabilize in Fe_3Sn_2[118,119]. Here, both macroscopic states can be accessed via a reversible process that overcomes the energy barrier by applying an electric or magnetic field. $CaBe_2Ge_2$ is another interesting example. Although it is centrosymmetric in character with a layered structure, inversion symmetry is broken locally in the middle of the two layers[120], inducing local DMI and leading to a stable skyrmionic crystal lattice[120]. $MnInP_2Te_6$ is predicted to stabilize a Bloch-type skyrmion lattice according to first-principles calculations and Monte-Carlo simulations[121]. Whereas $SrFeO_3$ has been shown to host skyrmions with a triple-q helical spin modulation[122].

These are encouraging examples towards the identification of suitable materials for hosting skyrmions for quantum operations. We expect further work in materials engineering assisted by machine learning to unlock more compounds[123,124,165]. A major challenge, however, is developing devices on high-quality epitaxial thin films, which may take time to reach optimal conditions for applications on an industrial scale. Meanwhile, thin lamellae can be cut from single crystals using a focused ion beam, following a similar routine to the sample preparation employed in transmission electron microscopy. Metallic top-gates and/or coplanar waveguides can be lithographically defined on hexagonal boron nitride (hBN) for electric field-tuned measurements.

B. Noise Mitigation

The interaction of the skyrmion qubit with the environmental degrees of freedom, however, leads to the collapse of the qubit's superposition into one definite state[125]. In practice, a skyrmion qubit is disrupted not only by interactions between its spin-whirls and the underlying magnet from which they emerge but also by the fluctuation of electromagnetic fields near the skyrmions. These forms of noise need to be combated with improved sample crystallinity, reduced damping, and dynamical decoupling from the environment by a set of pulses[126] in the multi-qubit gate[127].

Although magnetic thin films already exhibit the desired ultra-low Gilbert damping at room temperatures[128–131], the dependence of the damping coefficient on film thickness and temperature, especially at the sub-Kelvin qubit operational regime, is still not fully understood[132–134]. Furthermore, for better coherence times, it is imperative to focus on the development of cleaner magnetic samples and interfaces, without trading off qubit anharmonicity and scalability. High-quality layer-by-layer growth of heterostructures of skyrmion hosting perovskites such as $SrFeO_3$ is already possible by molecular beam epitaxy[135] and pulsed laser deposition[136]. Similar progress is expected to occur in other skyrmion hosts. Indeed, controlled layer-by-layer deposition methods are more promising than the sputtering techniques commonly employed in the field of skyrmionics, as they offer the potential for realizing low-defect heterostructures.

However, not just the magnetic thin film's quality is of critical importance. In the simplest skyrmion qubit platform, interlayer exchange interaction couples qubits via a nonmagnetic dielectric spacer, and logical states are adjusted by electric fields. Dielectrics with low loss at microwave frequencies are therefore crucial for high-coherence solid-state quantum computing platforms. Dielectric spacers between skyrmions are typically amorphous oxides with structural defects and their microscopic nature remains to be fully understood. However, hexagonal boron nitride (hBN) thin films offer a complementary platform to be suitably integrated into skyrmion qubit architectures[137]. Here, the microwave loss tangent of ultra-thin films of hBN is at most in the mid 10^{-6} range in the low-temperature regime. This is promising for building high-coherence quantum circuits with a substantial reduction of unwanted qubit cross-talk.

Besides strategies to mitigate quantum decoherence based on material engineering, alternative approaches built upon pulsed driving fields applied to the qubit might prove crucial. Dynamical decoupling[138] relies on a sequence of pulses inducing fast qubit flips that average out environmental fluctuations at a specific frequency. It emerges as a particularly encouraging strategy for addressing the challenges of decoherence, as it has been shown to improve coherence times[139,140] and can be integrated with quantum gates for a standard hybrid system[127]. Alternatively, for magnetic systems, monochromatic[141] and polychromatic[142] driving of the spin bath enhances qubit coherence times. Thus, for skyrmions in magnetic insulators where decoherence is dominated by magnetic noise, resonance frequency quantum control techniques can be employed on single qubits as well as on qubits linked up to form logic gates, to achieve optimal dynamical decoupling and improve coherence times.

C. Device Architecture

The integration of magnetic skyrmions into scalable quantum computing solid-state devices remains a challenge yet to be addressed. Utilizing a fundamental bottom-up approach in the design and engineering of quantum hardware involves tuning the skyrmion structure to produce the de-sired physical behavior. Positional control can be achieved by placing magnetic skyrmions in confined geometries in nanostructures[143–145]. Alternatively, defect engineering can offer precise energy landscapes to control the skyrmion trajectory and position[146,168]. Depending on the quantum architecture dimensionality, skyrmions are stabilized in 1D and 2D arrays of nanodomes with useful properties arising from the curved geometry[147]. Eventually, skyrmion qubits can be manufactured in large arrays using the lithographic technology employed in microelectronics. For true quantum computing, however, skyrmion qubits will have to link up in large arrays of memory units and logical gates, leading to scalability concerns.

The basic requirement for hardware here is the coupling of multiple skyrmions stabilized at ambient conditions and separated at the nanoscale, a feat for which encouraging results have already been reported using semiconductor-based capabilities[144]. Skyrmion-skyrmion interaction in 2D magnetic films[148,149] or bilayers[87,150] is sufficiently understood. Electric fields emerge as a new, powerful tool for a current-free low-power control of skyrmion dynamics. A reversible and reproducible skyrmion nucleation and annihilation mechanism has been discovered in a Pt/Co/oxide trilayer system[151,152] under electric field gating. The dynamic control of skyrmion helicity has been reported using voltage gating[153]. Finally, chiral skyrmions in multilayers X/CoFeB/MgO are manipulated under the influence of a magnetic field gradient using scanning tunneling microscopy (STM) tip[154]. Thus, the components of the suggested skyrmion qubit platform[3] are experimentally feasible with current technology.

D. New Qubit Designs and Outlook

The goal of this Perspective is to illustrate the potential magnetic skyrmions hold to exhibit controllable quantum behavior at the macroscale, allowing the implementation of quantum devices. We focused primarily on the conceptual framework and basic elements for the description of phenomena based on the quantum degree of skyrmion helicity. Domain walls with opposite chirality can also serve as the fundamental building blocks of a quantum computer[90,125] with similar decoherence time in the microsecond regime and operational frequency of a few GHz. Quantum phenomena within magnetic textures are crucial yet largely unexplored, presenting a promising avenue for further investigation and discovery. However, the relevance of topological magnetic textures to quantum technologies lies beyond gate-based quantum computing. Foremost, although magnetic skyrmions can execute specific tasks within a quantum processor, devices with multitasking capabilities rely on the coherent interaction of skyrmions with other degrees of freedom with complementary functionalities. In particular, hybrid quantum systems based on skyrmions coupled to microwave and optical photons, atoms, and individual electron and nuclear spins[155].

Moreover, magnetic skyrmions might prove applicable to unconventional quantum information processing, including

quantum reservoir computing based on quantum noise[156,157], adiabatic quantum computation[158,159], or methods that combine the advantages of different computational approaches[160]. Skyrmions have been proposed for topological quantum computation, as they induce topological superconductivity when proximized with conventional superconductors[161,162], forming skyrmion-vortex pairs hosting Majorana bound states (MBS). The experimental coupling of chiral magnetism and superconductivity[163] as well as the numerical demonstration of the non-Abelian statistics of MBS in this system[164] represent encouraging results in the pursuit of a scalable topological quantum computer.

In practice, the underexplored quantum platform involving topological magnetic textures reveals characteristics with the potential to significantly enhance the progress of quantum technologies. Skyrmion qubits depict the nascent connection between quantum applications and spin topology, offering exciting prospects for generating and preserving quantum information through magnetic quantum states.

V. ACKNOWLEDGMENTS

[1] M. A. Nielsen and I. L. Chuang, *Quantum Computation and Quantum Information: 10th Anniversary Edition* (Cambridge University Press, 2010).

[2] Y. Alexeev, D. Bacon, K. R. Brown, R. Calderbank, L. D. Carr, F. T. Chong, B. DeMarco, D. Englund, E. Farhi, B. Fefferman, A. V. Gorshkov, A. Houck, J. Kim, S. Kimmel, M. Lange, S. Lloyd, M. D. Lukin, D. Maslov, P. Maunz, C. Monroe, J. Preskill, M. Roetteler, M. J. Savage, and J. Thompson, "Quantum computer systems for scientific discovery," PRX Quantum 2, 017001 (2021).

[3] C. Psaroudaki and C. Panagopoulos, "Skyrmion qubits: A new class of quantum logic elements based on nanoscale magnetization," Phys. Rev. Lett. 127, 067201 (2021).

[4] A. Fert, N. Reyren, and V. Cros, "Magnetic skyrmions: advances in physics and potential applications," Nature Reviews Materials 2, 17031 (2017).

[5] Y. Tokura and N. Kanazawa, "Magnetic skyrmion materials," Chemical Reviews 121, 2857–2897 (2021), pMID: 33164494.

[6] A. Fert, V. Cros, and J. Sampaio, "Skyrmions on the track," Nature Nanotechnology 8, 152–156 (2013).

[7] D. Pinna, F. Abreu Araujo, J.-V. Kim, V. Cros, D. Querlioz, P. Bessiere, J. Droulez, and J. Grollier, "Skyrmion gas manipulation for probabilistic computing," Phys. Rev. Appl. 9, 064018 (2018).

[8] K. M. Song, J.-S. Jeong, B. Pan, X. Zhang, J. Xia, S. Cha, T.-E. Park, K. Kim, S. Finizio, J. Raabe, J. Chang, Y. Zhou, W. Zhao, W. Kang, H. Ju, and S. Woo, "Skyrmion-based artificial synapses for neuromorphic computing," Nature Electronics 3, 148–155 (2020).

[9] S. Heinze, K. von Bergmann, M. Menzel, J. Brede, A. Kubetzka, R. Wiesendanger, G. Bihlmayer, and S. Blügel, "Spontaneous atomic-scale magnetic skyrmion lattice in two dimensions," Nature Physics 7, 713–718 (2011).

[10] T. Kurumaji, T. Nakajima, M. Hirschberger, A. Kikkawa, Y. Yamasaki, H. Sagayama, H. Nakao, Y. Taguchi, T. hisa Arima, and Y. Tokura, "Skyrmion lattice with a giant topological hall effect in a frustrated triangular-lattice magnet," Science 365, 914–918 (2019).

[11] M. Hirschberger, T. Nakajima, S. Gao, L. Peng, A. Kikkawa, T. Kurumaji, M. Kriener, Y. Yamasaki, H. Sagayama, H. Nakao, K. Ohishi, K. Kakurai, Y. Taguchi, X. Yu, T.-h. Arima, and Y. Tokura, "Skyrmion phase and competing magnetic orders on a breathing kagomé lattice," Nature Communications 10, 5831 (2019).

[12] C. Psaroudaki, S. Hoffman, J. Klinovaja, and D. Loss, "Quantum dynamics of skyrmions in chiral magnets," Phys. Rev. X 7, 041045 (2017).

[13] R. Takashima, H. Ishizuka, and L. Balents, "Quantum skyrmions in two-dimensional chiral magnets," Phys. Rev. B 94, 134415 (2016).

[14] R. Wieser, "Self-consistent mean field theory studies of the thermodynamics and quantum spin dynamics of magnetic skyrmions," Journal of Physics: Condensed Matter 29, 175803 (2017).

[15] S.-Z. Lin and L. N. Bulaevskii, "Quantum motion and level quantization of a skyrmion in a pinning potential in chiral magnets," Phys. Rev. B 88, 060404 (2013).

[16] A. Mook, J. Klinovaja, and D. Loss, "Quantum damping of skyrmion crystal eigenmodes due to spontaneous quasiparticle decay," Phys. Rev. Research 2, 033491 (2020).

[17] A. Roldán-Molina, M. J. Santander, A. S. Nunez, and J. Fernández-Rossier, "Quantum fluctuations stabilize skyrmion textures," Phys. Rev. B 92, 245436 (2015).

[18] A. Derras-Chouk, E. M. Chudnovsky, and D. A. Garanin, "Quantum states of a skyrmion in a two-dimensional antiferromagnet," Phys. Rev. B 103, 224423 (2021).

[19] A. Derras-Chouk, E. M. Chudnovsky, and D. A. Garanin, "Quantum collapse of a magnetic skyrmion," Phys. Rev. B 98, 024423 (2018).

[20] C. Psaroudaki and D. Loss, "Quantum depinning of a magnetic skyrmion," Phys. Rev. Lett. 124, 097202 (2020).

[21] S. M. Vlasov, P. F. Bessarab, I. S. Lobanov, M. N. Potkina, V. M. Uzdin, and H. Jónsson, "Magnetic skyrmion annihilation by quantum mechanical tunneling," New Journal of Physics 22, 083013 (2020).

[22] S. A. Díaz and D. P. Arovas, "Quantum nucleation of skyrmions in magnetic films by inhomogeneous fields," in *Memorial Volume for Shoucheng Zhang* (2022) Chap. Chapter 2, pp. 19–33.

[23] O. M. Sotnikov, V. V. Mazurenko, J. Colbois, F. Mila, M. I. Katsnelson, and E. A. Stepanov, "Probing the topology of the quantum analog of a classical skyrmion," Phys. Rev. B 103, L060404 (2021).

[24] K. Mæland and A. Sudbø, "Quantum fluctuations in the order parameter of quantum skyrmion crystals," Phys. Rev. B 105, 224416 (2022).

[25] P. Siegl, E. Y. Vedmedenko, M. Stier, M. Thorwart, and T. Posske, "Controlled creation of quantum skyrmions," Phys. Rev. Research 4, 023111 (2022).

[26] V. Lohani, C. Hickey, J. Masell, and A. Rosch, "Quantum skyrmions in frustrated ferromagnets," Phys. Rev. X 9, 041063 (2019).

[27] K. Mæland and A. Sudbø, "Quantum topological phase transitions in skyrmion crystals," Phys. Rev. Research 4, L032025 (2022).

[28] H. Yuan, Y. Cao, A. Kamra, R. A. Duine, and P. Yan, "Quantum magnonics: When magnon spintronics meets quantum information science," Physics Reports 965, 1–74 (2022), quantum magnonics: When magnon spintronics meets quantum information science.

[29] D. Rugar, R. Budakian, H. J. Mamin, and B. W. Chui, "Single spin detection by magnetic resonance force microscopy," Nature 430, 329–332 (2004).

[30] D. Lachance-Quirion, S. P. Wolski, Y. Tabuchi, S. Kono, K. Usami, and Y. Nakamura, "Entanglement-based single-shot detection of a single magnon with a superconducting qubit," Science 367, 425–428 (2020).

[31] D. P. DiVincenzo, "The physical implementation of quantum computation," Fortschritte der Physik 48, 771–783 (2000).

[32] J. Clarke and F. K. Wilhelm, "Superconducting quantum bits," Nature 453, 1031–1042 (2008).

[33] C. Psaroudaki and C. Panagopoulos, "Skyrmion helicity: Quantization and quantum tunneling effects," Phys. Rev. B 106, 104422 (2022).

[34] Y. Tokura and N. Kanazawa, "Magnetic skyrmion materials," Chemical Reviews 121, 2857–2897 (2021), pMID: 33164494.

[35] C. D. Batista, S.-Z. Lin, S. Hayami, and Y. Kamiya, "Frustration and chiral orderings in correlated electron systems," Rep Prog Phys 79, 084504 (2016).

[36] H. Vakili, J.-W. Xu, W. Zhou, M. N. Sakib, M. G. Morshed, T. Hartnett, Y. Quessab, K. Litzius, C. T. Ma, S. Ganguly, M. R. Stan, P. V. Balachandran, G. S. D. Beach, S. J. Poon, A. D. Kent, and A. W. Ghosh,

"Skyrmionics—computing and memory technologies based on topological excitations in magnets," Journal of Applied Physics **130**, 070908 (2021).

[37]G. Finocchio and C. Panagopoulos, eds., *Magnetic Skyrmions and Their Applications*, Woodhead Publishing Series in Electronic and Optical Materials (Woodhead Publishing, 2021) p. xvii.

[38]N. Papanicolaou and T. Tomaras, "Dynamics of magnetic vortices," Nuclear Physics B **360**, 425–462 (1991).

[39]W. Jiang, G. Chen, K. Liu, J. Zang, S. G. te Velthuis, and A. Hoffmann, "Skyrmions in magnetic multilayers," Physics Reports **704**, 1–49 (2017), skyrmions in Magnetic Multilayers.

[40]L. D. Landau and E. Lifshitz, "On the theory of the dispersion of magnetic permeability in ferromagnetic bodies," Phys. Z. Sowjet. **8**, 153 (1935).

[41]O. A. Tretiakov, D. Clarke, G.-W. Chern, Y. B. Bazaliy, and O. Tchernyshyov, "Dynamics of domain walls in magnetic nanostrips," Phys. Rev. Lett. **100**, 127204 (2008).

[42]H. Ochoa and Y. Tserkovnyak, "Quantum skyrmionics," International Journal of Modern Physics B **33**, 1930005 (2019).

[43]D. P. DiVincenzo, "Quantum computation," Science **270**, 255–261 (1995).

[44]P. C. E. Stamp, "Quantum dynamics and tunneling of domain walls in ferromagnetic insulators," Phys. Rev. Lett. **66**, 2802–2805 (1991).

[45]H.-B. Braun, J. Kyriakidis, and D. Loss, "Macroscopic quantum tunneling of ferromagnetic domain walls," Phys. Rev. B **56**, 8129–8137 (1997).

[46]W. Wernsdorfer and R. Sessoli, "Quantum phase interference and parity effects in magnetic molecular clusters," Science **284**, 133–135 (1999).

[47]L. Thomas, F. Lionti, R. Ballou, D. Gatteschi, R. Sessoli, and B. Barbara, "Macroscopic quantum tunnelling of magnetization in a single crystal of nanomagnets," Nature **383**, 145–147 (1996).

[48]J. Brooke, T. F. Rosenbaum, and G. Aeppli, "Tunable quantum tunnelling of magnetic domain walls," Nature **413**, 610–613 (2001).

[49]E. M. Chudnovsky and J. Tejada, *Macroscopic Quantum Tunneling of the Magnetic Moment*, Cambridge Studies in Magnetism (Cambridge University Press, 1998).

[50]G. Blatter, M. V. Feigel'man, V. B. Geshkenbein, A. I. Larkin, and V. M. Vinokur, "Vortices in high-temperature superconductors," Rev. Mod. Phys. **66**, 1125–1388 (1994).

[51]J. Kyriakidis, D. Loss, and A. H. MacDonald, "Quantum dynamics of pseudospin solitons in double-layer quantum hall systems," Phys. Rev. Lett. **83**, 1411–1414 (1999).

[52]R. Zarzuela, S. Vélez, J. M. Hernandez, J. Tejada, and V. Novosad, "Quantum depinning of the magnetic vortex core in micron-size permalloy disks," Phys. Rev. B **85**, 180401 (2012).

[53]S. Luo and L. You, "Skyrmion devices for memory and logic applications," APL Materials **9**, 050901 (2021).

[54]Z. Yan, Y. Liu, Y. Guang, K. Yue, J. Feng, R. Lake, G. Yu, and X. Han, "Skyrmion-based programmable logic device with complete boolean logic functions," Phys. Rev. Appl. **15**, 064004 (2021).

[55]J. Grollier, D. Querlioz, K. Y. Camsari, K. Everschor-Sitte, S. Fukami, and M. D. Stiles, "Neuromorphic spintronics," Nature Electronics **3**, 360–370 (2020).

[56]K. Raab, M. A. Brems, G. Beneke, T. Dohi, J. Rothörl, F. Kammerbauer, J. H. Mentink, and M. Kläui, "Brownian reservoir computing realized using geometrically confined skyrmion dynamics," Nature Communications **13**, 6982 (2022).

[57]A. Bogdanov and A. Hubert, "Thermodynamically stable magnetic vortex states in magnetic crystals," Journal of Magnetism and Magnetic Materials **138**, 255–269 (1994).

[58]N. Nagaosa and Y. Tokura, "Topological properties and dynamics of magnetic skyrmions," Nature Nanotechnology **8**, 899–911 (2013).

[59]A. O. Leonov and M. Mostovoy, "Multiply periodic states and isolated skyrmions in an anisotropic frustrated magnet," Nature Communications **6**, 8275 (2015).

[60]X. Zhang, J. Xia, Y. Zhou, X. Liu, H. Zhang, and M. Ezawa, "Skyrmion dynamics in a frustrated ferromagnetic film and current-induced helicity locking-unlocking transition," Nature Communications **8**, 1717 (2017).

[61]P. E. Roy, R. M. Otxoa, and C. Moutafis, "Controlled anisotropic dynamics of tightly bound skyrmions in a synthetic ferrimagnet due to skyrmion deformation mediated by induced uniaxial in-plane anisotropy," Phys. Rev. B **99**, 094405 (2019).

[62]G. N. Kakazei, X. M. Liu, J. Ding, V. O. Golub, O. Y. Salyuk, R. V. Verba, S. A. Bunyaev, and A. O. Adeyeye, "Large four-fold magnetic anisotropy in two-dimensional modulated Ni80Fe20 films," Applied Physics Letters **107**, 232402 (2015).

[63]R. M. Bozorth, *Ferromagnetism* (Wiley-IEEE Press, 1978).

[64]M. N. Wilson, E. A. Karhu, A. S. Quigley, U. K. Rößler, A. B. Butenko, A. N. Bogdanov, M. D. Robertson, and T. L. Monchesky, "Extended elliptic skyrmion gratings in epitaxial mnsi thin films," Phys. Rev. B **86**, 144420 (2012).

[65]K. Shibata, J. Iwasaki, N. Kanazawa, S. Aizawa, T. Tanigaki, M. Shirai, T. Nakajima, M. Kubota, M. Kawasaki, H. S. Park, D. Shindo, N. Nagaosa, and Y. Tokura, "Large anisotropic deformation of skyrmions in strained crystal," Nature Nanotechnology **10**, 589–592 (2015).

[66]X. Yao, J. Chen, and S. Dong, "Controlling the helicity of magnetic skyrmions by electrical field in frustrated magnets," New Journal of Physics **22**, 083032 (2020).

[67]M. Kjaergaard, M. E. Schwartz, J. Braumüller, P. Krantz, J. I.-J. Wang, S. Gustavsson, and W. D. Oliver, "Superconducting qubits: Current state of play," Annual Review of Condensed Matter Physics **11**, 369–395 (2020).

[68]C. C. McGeoch, *Adiabatic Quantum Computation and Quantum Annealing* (Springer International Publishing, 2014).

[69]M. Brink, J. M. Chow, J. Hertzberg, E. Magesan, and S. Rosenblatt, "Device challenges for near term superconducting quantum processors: frequency collisions," in *2018 IEEE International Electron Devices Meeting (IEDM)* (2018) pp. 6.1.1–6.1.3.

[70]L. Landau, E. Lifshitz, E. Lifshits, and L. Pitaevskii, *Statistical Physics: Theory of the Condensed State*, Course of theoretical physics (Elsevier Science, 1980).

[71]T. Gilbert, "A phenomenological theory of damping in ferromagnetic materials," IEEE Transactions on Magnetics **40**, 3443–3449 (2004).

[72]R. K. Wangsness, "Sublattice effects in magnetic resonance," Phys. Rev. **91**, 1085–1091 (1953).

[73]F. Bloch, "Generalized theory of relaxation," Phys. Rev. **105**, 1206–1222 (1957).

[74]M. Kjaergaard, M. E. Schwartz, J. Braumüller, P. Krantz, J. I. Wang, S. Gustavsson, and W. D. Oliver, "Superconducting qubits: Current state of play," https://doi.org/10.1146/annurev-conmatphys-031119-050605 **11**, 369–395 (2020).

[75]C. Psaroudaki, P. Aseev, and D. Loss, "Quantum brownian motion of a magnetic skyrmion," Phys. Rev. B **100**, 134404 (2019).

[76]A. Caldeira and A. Leggett, "Quantum tunnelling in a dissipative system," Annals of Physics **149**, 374–456 (1983).

[77]E. M. Chudnovsky, O. Iglesias, and P. C. E. Stamp, "Quantum tunneling of domain walls in ferromagnets," Phys. Rev. B **46**, 5392–5404 (1992).

[78]G. Tatara, "Effective gauge field theory of spintronics," Physica E: Low-dimensional Systems and Nanostructures **106**, 208–238 (2019).

[79]T. Kikuchi and G. Tatara, "Spin dynamics with inertia in metallic ferromagnets," Phys. Rev. B **92**, 184410 (2015).

[80]H. M. Hurst, V. Galitski, and T. T. Heikkilä, "Electron-induced massive dynamics of magnetic domain walls," Phys. Rev. B **101**, 054407 (2020).

[81]F. Reyes-Osorio and B. K. Nikolic, "Anisotropic skyrmion mass induced by surrounding conduction electrons: A schwinger-keldysh field theory approach," (2023), arXiv:2302.04220.

[82]D. Capic, E. M. Chudnovsky, and D. A. Garanin, "Skyrmion mass from spin-phonon interaction," Phys. Rev. B **102**, 060404 (2020).

[83]A. Barenco, C. H. Bennett, R. Cleve, D. P. DiVincenzo, N. Margolus, P. Shor, T. Sleator, J. A. Smolin, and H. Weinfurter, "Elementary gates for quantum computation," Phys. Rev. A **52**, 3457–3467 (1995).

[84]C. M. Dawson and M. A. Nielsen, "The solovay-kitaev algorithm," Quantum Info. Comput. **6**, 81–95 (2006).

[85]D. C. McKay, C. J. Wood, S. Sheldon, J. M. Chow, and J. M. Gambetta, "Efficient z gates for quantum computing," Phys. Rev. A **96**, 022330 (2017).

[86]J. Xia, X. Zhang, X. Liu, Y. Zhou, and M. Ezawa, "Universal quantum computation based on nanoscale skyrmion helicity qubits in frustrated magnets," Phys. Rev. Lett. **130**, 106701 (2023).

[87]W. Koshibae and N. Nagaosa, "Theory of skyrmions in bilayer systems," Scientific Reports **7**, 42645 (2017).

[88]S. A. Díaz, T. Hirosawa, D. Loss, and C. Psaroudaki, "Spin wave radiation by a topological charge dipole," Nano Letters **20**, 6556–6562 (2020), pMID: 32812768.

[89] N. Schuch and J. Siewert, "Natural two-qubit gate for quantum computation using the XY interaction," Phys. Rev. A **67**, 032301 (2003).

[90] J. Zou, S. Bosco, B. Pal, S. S. P. Parkin, J. Klinovaja, and D. Loss, "Domain wall qubits on magnetic racetracks," (2022), arXiv:2212.12019.

[91] M. Fukami, D. R. Candido, D. D. Awschalom, and M. E. Flatté, "Opportunities for long-range magnon-mediated entanglement of spin qubits via on- and off-resonant coupling," PRX Quantum **2**, 040314 (2021).

[92] T. Hirosawa, A. Mook, J. Klinovaja, and D. Loss, "Magnetoelectric cavity magnonics in skyrmion crystals," PRX Quantum **3**, 040321 (2022).

[93] G. Vidal, K. Hammerer, and J. I. Cirac, "Interaction cost of nonlocal gates," Phys. Rev. Lett. **88**, 237902 (2002).

[94] M. M. Midzor, P. E. Wigen, D. Pelekhov, W. Chen, P. C. Hammel, and M. L. Roukes, "Imaging mechanisms of force detected FMR microscopy," Journal of Applied Physics **87**, 6493–6495 (2000), https://pubs.aip.org/aip/jap/article-pdf/87/9/6493/10606166/6493_1_online.pdf.

[95] E. Arima, Y. Naitoh, Y. J. Li, S. Yoshimura, H. Saito, H. Nomura, R. Nakatani, and Y. Sugawara, "Magnetic force microscopy using tip magnetization modulated by ferromagnetic resonance," Nanotechnology **26**, 125701 (2015).

[96] M. Sapozhnikov, D. Tatarskiy, and V. Mironov, "Creating and detecting a magnetic bimeron by magnetic force microscope probe," Journal of Magnetism and Magnetic Materials **549**, 169043 (2022).

[97] H. J. Hug, *Magnetic Skyrmions and Their Applications: Chapter 4 - Mapping the magnetic field of skyrmions and spin spirals by scanning probe microscopy* (Woodhead Publishing, 2021).

[98] S. Pöllath, A. Aqeel, A. Bauer, C. Luo, H. Ryll, F. Radu, C. Pfleiderer, G. Woltersdorf, and C. H. Back, "Ferromagnetic resonance with magnetic phase selectivity by means of resonant elastic x-ray scattering on a chiral magnet," Phys. Rev. Lett. **123**, 167201 (2019).

[99] B. Satywali, V. P. Kravchuk, L. Pan, M. Raju, S. He, F. Ma, A. P. Petrović, M. Garst, and C. Panagopoulos, "Microwave resonances of magnetic skyrmions in thin film multilayers," nature.com.remotexs.ntu.edu.sgmunications 2021 12:1 **12**, 1–8 (2021).

[100] Y. Dovzhenko, F. Casola, S. Schlotter, T. X. Zhou, F. Büttner, R. L. Walsworth, G. S. D. Beach, and A. Yacoby, "Magnetostatic twists in room-temperature skyrmions explored by nitrogen-vacancy center spin texture reconstruction," nature.com.remotexs.ntu.edu.sgmunications 2018 9:1 **9**, 1–7 (2018).

[101] A. R. Stuart, K. L. Livesey, and K. S. Buchanan, "Fast, semianalytical approach to obtain the stray magnetic field above a magnetic skyrmion," Phys. Rev. B **105**, 144430 (2022).

[102] E. Marchiori, L. Ceccarelli, N. Rossi, L. Lorenzelli, C. L. Degen, and M. Poggio, "Nanoscale magnetic field imaging for 2d materials," Nature Reviews Physics 2021 4:1 **4**, 49–60 (2021).

[103] J. R. Rabeau, A. Stacey, A. Rabeau, S. Prawer, F. Jelezko, I. Mirza, and J. Wrachtrup, "Single nitrogen vacancy centers in chemical vapor deposited diamond nanocrystals," Nano Letters **7**, 3433–3437 (2007), pMID: 17902725, https://doi.org/10.1021/nl0719271.

[104] S. Pezzagna, B. Naydenov, F. Jelezko, J. Wrachtrup, and J. Meijer, "Creation efficiency of nitrogen-vacancy centres in diamond," New Journal of Physics **12**, 065017 (2010).

[105] E. Bernardi, R. Nelz, S. Sonusen, and E. Neu, "Nanoscale sensing using point defects in single-crystal diamond: Recent progress on nitrogen vacancy center-based sensors," Crystals **7** (2017), 10.3390/cryst7050124.

[106] N. Jiang, Y. Nii, H. Arisawa, E. Saitoh, and Y. Onose, "Electric current control of spin helicity in an itinerant helimagnet," Nature Communications 2020 11:1 **11**, 1–6 (2020).

[107] I. Lima Fernandes, S. Blügel, and S. Lounis, "Spin-orbit enabled all-electrical readout of chiral spin-textures," Nature Communications **13**, 1576 (2022).

[108] V. Chandragiri, K. K. Iyer, and E. V. Sampathkumaran, "Magnetic behavior of gd3ru4al12, a layered compound with distorted kagomé net," Journal of Physics: Condensed Matter **28**, 286002 (2016).

[109] M. Hirschberger, T. Nakajima, S. Gao, L. Peng, A. Kikkawa, T. Kurumaji, M. Kriener, Y. Yamasaki, H. Sagayama, H. Nakao, K. Ohishi, K. Kakurai, Y. Taguchi, X. Yu, T.-H. Arima, and Y. Tokura, "Skyrmion phase and competing magnetic orders on a breathing kagomé lattice," Nature communications **10**, 5831 (2019).

[110] C. Boragno, M. Bonansinga, and F. Nava, "Electrical and magnetic properties if ersi2 and gdsi2 alloy thin films," Solid State Communications **92**, 515–518 (1994).

[111] P. Sonnet, L. Stauffer, S. Saintenoy, C. Pirri, P. Wetzel, G. Gewinner, and C. Minot, "Electronic and atomic structure of two-dimensional ersi$_2$ (1 × 1)-h on si(111)," Phys. Rev. B **56**, 15171–15179 (1997).

[112] I. Auneau, G. Fraga, D. Gignoux, D. Schmitt, and F. Zhang, "Magnetic phase diagram of tbga$_2$," Physica B: Condensed Matter **212**, 351–356 (1995).

[113] T. Okubo, S. Chung, and H. Kawamura, "Multiple-q states and the skyrmion lattice of the triangular-lattice heisenberg antiferromagnet under magnetic fields," Phys. Rev. Lett. **108**, 017206 (2012).

[114] H. Yamaguchi, S. Kimura, M. Hagiwara, Y. Nambu, S. Nakatsuji, Y. Maeno, and K. Kindo, "High-field electron spin resonance in the two-dimensional triangular-lattice antiferromagnet niga$_2$s$_4$," Phys. Rev. B **78**, 180404 (2008).

[115] S. Nakatsuji, Y. Nambu, H. Tonomura, O. Sakai, S. Jonas, C. Broholm, H. Tsunetsugu, Y. Qiu, and Y. Maeno, "Spin disorder on a triangular lattice," Science **309**, 1697–1700 (2005).

[116] S. Nakatsuji, Y. Nambu, K. Onuma, S. Jonas, C. Broholm, and Y. Maeno, "Coherent behaviour without magnetic order of the triangular lattice antiferromagnet niga2s4," Journal of Physics: Condensed Matter **19**, 145232 (2007).

[117] H. Takeya, K. Ishida, K. Kitagawa, Y. Ihara, K. Onuma, Y. Maeno, Y. Nambu, S. Nakatsuji, D. E. MacLaughlin, A. Koda, and R. Kadono, "Spin dynamics and spin freezing behavior in the two-dimensional antiferromagnet Niga$_2$s$_4$ revealed by ga-nmr, nqr and μSR measurements," Phys. Rev. B **77**, 054429 (2008).

[118] Z. Hou, Q. Zhang, G. Xu, S. Zhang, C. Gong, B. Ding, H. Li, F. Xu, Y. Yao, E. Liu, G. Wu, X. X. Zhang, and W. Wang, "Manipulating the topology of nanoscale skyrmion bubbles by spatially geometric confinement," ACS Nano **13**, 922–929 (2019).

[119] Z. Hou, Q. Zhang, X. Zhang, G. Xu, J. Xia, B. Ding, H. Li, S. Zhang, N. M. Batra, P. M. Costa, E. Liu, G. Wu, M. Ezawa, X. Liu, Y. Zhou, X. Zhang, and W. Wang, "Current-induced helicity reversal of a single skyrmionic bubble chain in a nanostructured frustrated magnet," Advanced Materials **32**, 1904815 (2020).

[120] S.-Z. Lin, "Skyrmion lattice in centrosymmetric magnets with local dzyaloshinsky-moriya interaction," (2021), arXiv:2112.12850.

[121] W. Du, K. Dou, Y. Dai, B. Huang, and Y. Ma, "Bloch-type magnetic skyrmions in two-dimensional lattice," (2023), arXiv:2304.00671.

[122] S. Ishiwata, T. Nakajima, J.-H. Kim, D. S. Inosov, N. Kanazawa, J. S. White, J. L. Gavilano, R. Georgii, K. M. Seemann, G. Brandl, P. Manuel, D. D. Khalyavin, S. Seki, Y. Tokunaga, M. Kinoshita, Y. W. Long, Y. Kaneko, Y. Taguchi, T. Arima, B. Keimer, and Y. Tokura, "Emergent topological spin structures in the centrosymmetric cubic perovskite srfeo$_3$," Phys. Rev. B **101**, 134406 (2020).

[123] H. A. Merker, H. Heiberger, L. Nguyen, T. Liu, Z. Chen, N. Andrejevic, N. C. Drucker, R. Okabe, S. E. Kim, Y. Wang, T. Smidt, and M. Li, "Machine learning magnetism classifiers from atomic coordinates," iScience **25**, 105192 (2022).

[124] J. Greitemann, K. Liu, L. D. C. Jaubert, H. Yan, N. Shannon, and L. Pollet, "Identification of emergent constraints and hidden order in frustrated magnets using tensorial kernel methods of machine learning," Phys. Rev. B **100**, 174408 (2019).

[125] S. Takei and M. Mohseni, "Quantum control of topological defects in magnetic systems," Phys. Rev. B **97**, 064401 (2018).

[126] L. Viola, S. Lloyd, and E. Knill, "Universal control of decoupled quantum systems," Phys. Rev. Lett. **83**, 4888–4891 (1999).

[127] T. van der Sar, Z. H. Wang, M. S. Blok, H. Bernien, T. H. Taminiau, D. M. Toyli, D. A. Lidar, D. D. Awschalom, R. Hanson, and V. V. Dobrovitski, "Decoherence-protected quantum gates for a hybrid solid-state spin register," Nature **484**, 82–86 (2012).

[128] L. Soumah, N. Beaulieu, L. Qassym, C. Carrétéro, E. Jacquet, R. Lebourgeois, J. B. Youssef, P. Bortolotti, V. Cros, and A. Anane, "Ultra-low damping insulating magnetic thin films get perpendicular," Nature Communications 2018 9:1 **9**, 1–6 (2018).

[129] C. Hauser, T. Richter, N. Homonnay, C. Eisenschmidt, M. Qaid, H. Deniz, D. Hesse, M. Sawicki, S. G. Ebbinghaus, and G. Schmidt, "Yttrium iron garnet thin films with very low damping obtained by recrystallization of

amorphous material," Scientific Reports 2016 6:1 **6**, 1–8 (2016).

[130] Q. Qin, S. He, W. Song, P. Yang, Q. Wu, Y. P. Feng, and J. Chen, "Ultra-low magnetic damping of perovskite la0.7sr0.3mno3 thin films," Applied Physics Letters **110** (2017), 10.1063/1.4978431/32760.

[131] H. Chang, P. Li, W. Zhang, T. Liu, A. Hoffmann, L. Deng, and M. Wu, "Nanometer-thick yttrium iron garnet films with extremely low damping," IEEE Magnetics Letters **5** (2014), 10.1109/LMAG.2014.2350958.

[132] S. Guo, B. McCullian, P. C. Hammel, and F. Yang, "Low damping at few-k temperatures in y3fe5o12 epitaxial films isolated from gd3ga5o12 substrate using a diamagnetic y3sc2.5al2.5o12 spacer," Journal of Magnetism and Magnetic Materials **562**, 169795 (2022).

[133] V. Haspot, P. Noël, J. P. Attané, L. Vila, M. Bibes, A. Anane, and A. Barthélémy, "Temperature dependence of the gilbert damping of la0.7sr0.3mno3 thin films," Physical Review Materials **6**, 024406 (2022).

[134] L. Jin, Y. Wang, G. Lu, J. Li, Y. He, Z. Zhong, and H. Zhang, "Temperature dependence of spin-wave modes and gilbert damping in lanthanum-doped yttrium-iron-garnet films," AIP Advances **9**, 25301 (2019).

[135] D. Hong, C. Liu, J. Pearson, and A. Bhattacharya, "Epitaxial growth of high quality SrFeO3 films on (001) oriented (LaAlO3)0.3(Sr2TaAlO6)0.7," Applied Physics Letters **111**, 232408 (2017), https://pubs.aip.org/aip/apl/article-pdf/doi/10.1063/1.5002672/14507417/232408_1_online.pdf.

[136] J. Chang, J.-W. Lee, and S.-K. Kim, "Layer-by-layer growth of srfeo3-δ thin films on atomically flat single-terminated srruo3/srtio3 (111) surfaces," Journal of Crystal Growth **312**, 621–623 (2010).

[137] J. I. Wang, M. A. Yamoah, Q. Li, A. H. Karamlou, T. Dinh, B. Kannan, J. Braumüller, D. Kim, A. J. Melville, S. E. Muschinske, B. M. Niedzielski, K. Serniak, Y. Sung, R. Winik, J. L. Yoder, M. E. Schwartz, K. Watanabe, T. Taniguchi, T. P. Orlando, S. Gustavsson, P. Jarillo-Herrero, and W. D. Oliver, "Hexagonal boron nitride as a low-loss dielectric for superconducting quantum circuits and qubits," Nature Materials 2022 21:4 **21**, 398–403 (2022).

[138] L. Viola and S. Lloyd, "Dynamical suppression of decoherence in two-state quantum systems," Phys. Rev. A **58**, 2733–2744 (1998).

[139] J. Bylander, S. Gustavsson, F. Yan, F. Yoshihara, K. Harrabi, G. Fitch, D. G. Cory, Y. Nakamura, J.-S. Tsai, and W. D. Oliver, "Noise spectroscopy through dynamical decoupling with a superconducting flux qubit," Nature Physics **7**, 565–570 (2011).

[140] G. de Lange, Z. H. Wang, D. Ristè, V. V. Dobrovitski, and R. Hanson, "Universal dynamical decoupling of a single solid-state spin from a spin bath," Science **330**, 60–63 (2010), https://www.science.org/doi/pdf/10.1126/science.1192739x.

[141] J. F. Barry, J. M. Schloss, E. Bauch, M. J. Turner, C. A. Hart, L. M. Pham, and R. L. Walsworth, "Sensitivity optimization for nv-diamond magnetometry," Rev. Mod. Phys. **92**, 015004 (2020).

[142] M. Joos, D. Bluvstein, Y. Lyu, D. Weld, and A. Bleszynski Jayich, "Protecting qubit coherence by spectrally engineered driving of the spin environment," npj Quantum Information **8**, 47 (2022).

[143] O. Boulle, J. Vogel, H. Yang, S. Pizzini, D. de Souza Chaves, A. Locatelli, T. O. Menteş, A. Sala, L. D. Buda-Prejbeanu, O. Klein, M. Belmeguenai, Y. Roussigné, A. Stashkevich, S. M. Chérif, L. Aballe, M. Foerster, M. Chshiev, S. Auffret, I. M. Miron, and G. Gaudin, "Room-temperature chiral magnetic skyrmions in ultrathin magnetic nanostructures," Nature Nanotechnology **11**, 449–454 (2016).

[144] P. Ho, A. K. Tan, S. Goolaup, A. G. Oyarce, M. Raju, L. Huang, A. Soumyanarayanan, and C. Panagopoulos, "Geometrically tailored skyrmions at zero magnetic field in multilayered nanostructures," Phys. Rev. Appl. **11**, 024064 (2019).

[145] X. Zhao, C. Jin, C. Wang, H. Du, J. Zang, M. Tian, R. Che, and Y. Zhang, "Direct imaging of magnetic field-driven transitions of skyrmion cluster states in fege nanodisks," Proceedings of the National Academy of Sciences **113**, 4918–4923 (2016), https://www.pnas.org/doi/pdf/10.1073/pnas.1600197113.

[146] I. Lima Fernandes, J. Bouaziz, S. Blügel, and S. Lounis, "Universality of defect-skyrmion interaction profiles," Nature Communications **9**, 4395 (2018).

[147] F. Tejo, D. Toneto, S. Oyarzún, J. Hermosilla, C. S. Danna, J. L. Palma, R. B. da Silva, L. S. Dorneles, and J. C. Denardin, "Stabilization of magnetic skyrmions on arrays of self-assembled hexagonal nanodomes for magnetic recording applications," ACS Applied Materials & Interfaces **12**, 53454–53461 (2020).

[148] X. Zhang, G. P. Zhao, H. Fangohr, J. P. Liu, W. X. Xia, J. Xia, and F. J. Morvan, "Skyrmion-skyrmion and skyrmion-edge repulsions in skyrmion-based racetrack memory," Scientific Reports **5**, 7643 (2015).

[149] D. Capic, D. A. Garanin, and E. M. Chudnovsky, "Skyrmion–skyrmion interaction in a magnetic film," Journal of Physics: Condensed Matter **32**, 415803 (2020).

[150] X. Zhang, Y. Zhou, and M. Ezawa, "Magnetic bilayer-skyrmions without skyrmion hall effect," Nature Communications **7**, 10293 (2016).

[151] M. Schott, A. Bernand-Mantel, L. Ranno, S. Pizzini, J. Vogel, H. Béa, C. Baraduc, S. Auffret, G. Gaudin, and D. Givord, "The skyrmion switch: Turning magnetic skyrmion bubbles on and off with an electric field," Nano Letters **17**, 3006–3012 (2017).

[152] P.-J. Hsu, A. Kubetzka, A. Finco, N. Romming, K. von Bergmann, and R. Wiesendanger, "Electric-field-driven switching of individual magnetic skyrmions," Nature Nanotechnology **12**, 123–126 (2017).

[153] T. Srivastava, M. Schott, R. Juge, V. Křižáková, M. Belmeguenai, Y. Roussigné, A. Bernand-Mantel, L. Ranno, S. Pizzini, S.-M. Chérif, A. Stashkevich, S. Auffret, O. Boulle, G. Gaudin, M. Chshiev, C. Baraduc, and H. Béa, "Large-voltage tuning of dzyaloshinskii–moriya interactions: A route toward dynamic control of skyrmion chirality," Nano Letters **18**, 4871–4877 (2018), pMID: 29924621, https://doi.org/10.1021/acs.nanolett.8b01502.

[154] A. Casiraghi, H. Corte-León, M. Vafaee, F. Garcia-Sanchez, G. Durin, M. Pasquale, G. Jakob, M. Kläui, and O. Kazakova, "Individual skyrmion manipulation by local magnetic field gradients," Communications Physics **2**, 145 (2019).

[155] A. A. Clerk, K. W. Lehnert, P. Bertet, J. R. Petta, and Y. Nakamura, "Hybrid quantum systems with circuit quantum electrodynamics," Nature Physics **16**, 257–267 (2020).

[156] K. Fujii and K. Nakajima, "Harnessing disordered-ensemble quantum dynamics for machine learning," Phys. Rev. Appl. **8**, 024030 (2017).

[157] J. Chen, H. I. Nurdin, and N. Yamamoto, "Temporal information processing on noisy quantum computers," Phys. Rev. Appl. **14**, 024065 (2020).

[158] E. Farhi, J. Goldstone, S. Gutmann, and M. Sipser, "Quantum computation by adiabatic evolution," (2000), arXiv:quant-ph/0001106.

[159] E. Farhi, J. Goldstone, S. Gutmann, J. Lapan, A. Lundgren, and D. Preda, "A quantum adiabatic evolution algorithm applied to random instances of an np-complete problem," Science **292**, 472–475 (2001), https://www.science.org/doi/pdf/10.1126/science.1057726.

[160] R. Barends, A. Shabani, L. Lamata, J. Kelly, A. Mezzacapo, U. L. Heras, R. Babbush, A. G. Fowler, B. Campbell, Y. Chen, Z. Chen, B. Chiaro, A. Dunsworth, E. Jeffrey, E. Lucero, A. Megrant, J. Y. Mutus, M. Neeley, C. Neill, P. J. J. O'Malley, C. Quintana, P. Roushan, D. Sank, A. Vainsencher, J. Wenner, T. C. White, E. Solano, H. Neven, and J. M. Martinis, "Digitized adiabatic quantum computing with a superconducting circuit," Nature **534**, 222–226 (2016).

[161] G. Yang, P. Stano, J. Klinovaja, and D. Loss, "Majorana bound states in magnetic skyrmions," Phys. Rev. B **93**, 224505 (2016).

[162] M. Garnier, A. Mesaros, and P. Simon, "Topological superconductivity with deformable magnetic skyrmions," Communications Physics **2**, 126 (2019).

[163] A. P. Petrović, M. Raju, X. Y. Tee, A. Louat, I. Maggio-Aprile, R. M. Menezes, M. J. Wyszyński, N. K. Duong, M. Reznikov, C. Renner, M. V. Milošević, and C. Panagopoulos, "Skyrmion-(anti)vortex coupling in a chiral magnet-superconductor heterostructure," Phys. Rev. Lett. **126**, 117205 (2021).

[164] J. Nothhelfer, S. A. Díaz, S. Kessler, T. Meng, M. Rizzi, K. M. D. Hals, and K. Everschor-Sitte, "Steering majorana braiding via skyrmion-vortex pairs: A scalable platform," Phys. Rev. B **105**, 224509 (2022).

[165] I. A. Iakovlev, O. M. Sotnikov, and V. V. Mazurenko, "Supervised learning approach for recognizing magnetic skyrmion phases," Phys. Rev. B **98**, 174411 (2018).

[166] M. H. Devoret and R. J. Schoelkopf, "Superconducting circuits for quantum information: An outlook," Science **339**, 1169–1174 (2013), https://www.science.org/doi/pdf/10.1126/science.1231930.

[167] S.-Z. Lin and S. Hayami, "Ginzburg-landau theory for skyrmions in inversion-symmetric magnets with competing interactions," Phys. Rev. B **93**, 064430 (2016).

[168] I. G. Arjana, I. Lima Fernandes, J. Chico, and S. Lounis, "Sub-nanoscale atom-by-atom crafting of skyrmion-defect interaction profiles," Scientific Reports **10**, 14655 (2020).